Biophysical models reveal the relative importance of transporter proteins and impermeant anions in chloride homeostasis

Kira M. Düsterwald[1], Christopher B. Currin[1], Richard J. Burman[1], Colin J. Akerman[2], Alan R. Kay[3], Joseph V. Raimondo[1]

[1]Division of Cell Biology, Department of Human Biology, Neuroscience Institute and Institute of Infectious Disease and Molecular Medicine, Faculty of Health Sciences, University of Cape Town, Cape Town, South Africa

[2]Department of Pharmacology, University of Oxford, Oxford, United Kingdom

[3]Department of Biology, University of Iowa, Iowa City, IA, USA

Correspondence:
Joseph V. Raimondo
email: joseph.raimondo@uct.ac.za

and

Alan R. Kay
email: alan-kay@uiowa.edu

Running Title
The cellular determinants of Cl^- driving force in the nervous system.

Keywords
Chloride, cation-chloride cotransport, impermeant anions, KCC2, Na^+/K^+ ATPase, synaptic inhibition, GABA, cell size

Acknowledgements

We would like to thank Juha Voipio for critically reading the manuscript and providing helpful comments and suggestions. This work was supported by the Mandela Rhodes Foundation (KMD and RJB), a DAAD-NRF scholarship (CBC), a Newton Advanced Fellowship (JVR) and the Blue Brain Project.

Abstract

Fast synaptic inhibition in the nervous system depends on the transmembrane flux of Cl^- ions based on the neuronal Cl^- driving force. Established theories regarding the determinants of Cl^- driving force have recently been questioned. Here we present biophysical models of Cl^- homeostasis using the pump-leak model. Using novel numerical and analytic solutions, we demonstrate that the Na^+/K^+ ATPase, ion conductances, impermeant anions, electrodiffusion, water fluxes and cation-chloride cotransporters (CCCs) play roles in setting the Cl^- driving force. We show that impermeant anions have a negligible effect on the driving force for Cl^- either locally or cell-wide. While impermeant anions can contribute to setting the intracellular Cl^- concentration in neurons, they can only affect Cl^- driving force by modifying the activity of active transport mechanisms (i.e. the Na^+/K^+ ATPase). In contrast, we demonstrate that CCCs are well-suited for modulating Cl^- driving force and hence inhibitory signaling in neurons.

Introduction

Fast synaptic inhibition in the nervous system is primarily mediated by chloride (Cl^-) permeable type A γ-aminobutyric acid receptors ($GABA_A$Rs) and glycine receptors (GlyRs) (Farrant and Kaila, 2007). Together with the neuronal membrane potential, the transmembrane gradient for Cl^- sets the driving force for Cl^- flux across these receptors and hence controls the properties of $GABA_A$R and GlyR mediated signaling within neural networks. Modification of intraneuronal Cl^- concentration, and hence Cl^- driving force, has been shown to play a causative role in multiple neurological diseases including epilepsy, chronic pain, schizophrenia and autism (Huberfeld et al., 2007; Hyde et al., 2011; Price et al., 2009; Rivera et al., 2004; Tyzio et al., 2014). Similarly, intracellular Cl^- is thought to be modulated as a function of brain development to ensure that GABAergic transmission contributes optimally to the construction of neural circuits (Ben-Ari, 2002). Given the central importance of Cl^- for brain function and dysfunction, the cellular mechanisms that control the transmembrane Cl^- gradient and driving force for $GABA_A$Rs and GlyRs are of considerable interest.

Plasmalemmal Cl^- transporters, and in particular cation-chloride cotransporters (CCCs), are understood to be the major mechanism by which neurons regulate the driving force for Cl^- permeable anion channels (Kaila et al., 2014). Recently it has been suggested that it is in fact local impermeant anions that control local Cl^- concentration and the driving force for $GABA_A$R and GlyR signaling (Glykys et al., 2014), rather than the CCCs. The majority of intracellular anions are impermeant to the neuronal membrane; these include ribo- and deoxynucleotides, intracellular proteins and metabolites (Burton, 1983). Impermeant anions induce what is known as the Donnan (or Gibbs-Donnan) effect (Hill, 1956; Sperelakis, 2012) - an uneven distribution of charged molecules across the membrane which is osmotically unstable. Without active ion transport to counter this effect, neurons would rapidly swell and burst (Kay, 2017). All animal cells, including neurons, maintain cell volume in the presence of impermeant anions by using the Na^+/K^+ ATPase to pump Na^+ out of the cell and K^+ in, along with the passive movement of water and permeable ions (Armstrong, 2003; Kay, 2017; Liang et al., 2007; Tosteson and Hoffman, 1960). This pump-leak mechanism, whilst stabilizing cell volume, also establishes the negative resting membrane potential and transmembrane Na^+ and K^+ transmembrane gradients, which serve as an energy source for the coupled transport of other molecules, including Cl^- by CCCs. In the absence of active Cl^- transport the intracellular Cl^- concentration is set by the membrane potential; i.e. the Nernst potential of Cl^- ($E_{Cl} = \frac{RT}{F} \ln \frac{Cl_i}{Cl_o}$) is equal to the transmembrane potential (V).

The transmembrane Cl^- gradient and the driving force ($DF=V-E_{Cl}$) for Cl^- permeable ion channels are therefore the outcome of multiple, dynamically interacting cellular mechanisms, which makes experimental investigation of the determinants underlying Cl^- homeostasis difficult. As a result, computational models based on established biophysical first principles are a productive means for exploring the possible roles of various cellular mechanisms (Na^+/K^+ ATPase, impermeant anions, CCCs, ion conductances and electrodiffusion) in generating the local driving force for Cl^-. To date computational models of Cl^- homeostasis have not combined all of these parameters in a single, multi-compartment formulation. Nor have they included the water fluxes, driven by transmembrane osmotic differences, which change cell volume. Here, we establish numerical and novel analytic solutions for a model of Cl^- homeostasis to explore the determinants of the neuronal driving force for Cl^-. We demonstrate that the baseline Cl^- concentration is a product of the interaction of multiple fundamental cell parameters: Na^+/K^+ ATPase activity, the average charge of impermeant anions, ion conductances, CCCs and water permeability.

We find that while impermeant anions can contribute to setting the intracellular Cl^- concentration in neurons, they cannot directly affect the driving force for Cl^- without modifying the activity of active transport mechanisms (i.e. the Na^+/K^+ ATPase). Even in the context of indirect interactions, we show that impermeable anions have a negligible effect on the driving force for Cl^- either locally or cell-wide

(< 1 mV). The ability of impermeant anions to generate these small modifications to Cl^- driving force requires the presence of CCCs and is due to changes in Na^+/K^+ ATPase activity via impermeant anion driven modification of the transmembrane Na^+ gradient.

In contrast, we demonstrate that CCCs are well-suited as the only known mechanism for modulating Cl^- driving force and hence the properties of inhibitory signaling in the nervous system. CCCs selectively regulate substantial changes in the driving force for Cl^-, consistent with a meta-analysis generated using a systematic review of available experimental data, which shows a strong correlation between the activity of the specific CCC, KCC2, and neuronal Cl^- concentration. Finally, using multicompartment models we demonstrate that the ability of CCCs to specifically modulate Cl^- at a local level depends on the characteristics of Cl^- electrodiffusion in the structure concerned.

Our biophysical models therefore provide a powerful framework for examining Cl^- homeostasis in neurons and have enabled us to demonstrate the respective roles of CCCs and impermeant anions in Cl^- regulation.

Results

<u>A biophysical model based on the pump-leak mechanism demonstrates the importance of the sodium-potassium ATPase for setting transmembrane ion gradients including chloride.</u>

To compare the effects of impermeant anions and Cl^- cotransport on Cl^- homeostasis we first developed a single compartment model based on the pump-leak formulation (Kay, 2017; Tosteson and Hoffman, 1960) (**Fig. 1a**). This model, defined by a set of differential equations, incorporated mathematical representations of the three major permeable ion species Cl^-, K^+, Na^+ as well as impermeant anions (X^z) with average charge z. Permeable ions could move across the cellular membrane via passive conductances according to each ion's respective electrochemical gradient. Further, active transport of Na^+ and K^+ by the Na^+/K^+ ATPase and cotransport of Cl^- and K^+ by the cation-chloride cotransporter KCC2 with a non-zero conductance g_{KCC2} of 2×10^{-3} S/dm^2 unless otherwise stated were included. Finally, our formulation accounted for the dynamics of cell volume (w), osmolarity (Π) and transmembrane voltage (V) (see Materials and Methods). Importantly, regardless of initial starting concentrations of permeant or impermeant ions, cell volume or V, the model converged to stable fixed points without needing to include any means for 'sensing' ion concentration, volume or voltage. In the case of permeable ions, initial concentrations did not even determine the final cellular volume. For example, despite initiating the model with different starting concentrations of Cl^- (1, 15, 40 and 60 mM respectively, **Fig. 1b**), the Cl^- concentration always converged to the same stable concentration of 5.2 mM, a typical baseline Cl^- concentration for adult neurons, and volume always converged to 2.0 pL, a typical volume for hippocampal neurons (Ambros-Ingerson and Holmes, 2005). The model is robust in the sense that its convergence to a stable steady state does not depend on a narrow set of parameters and initial values.

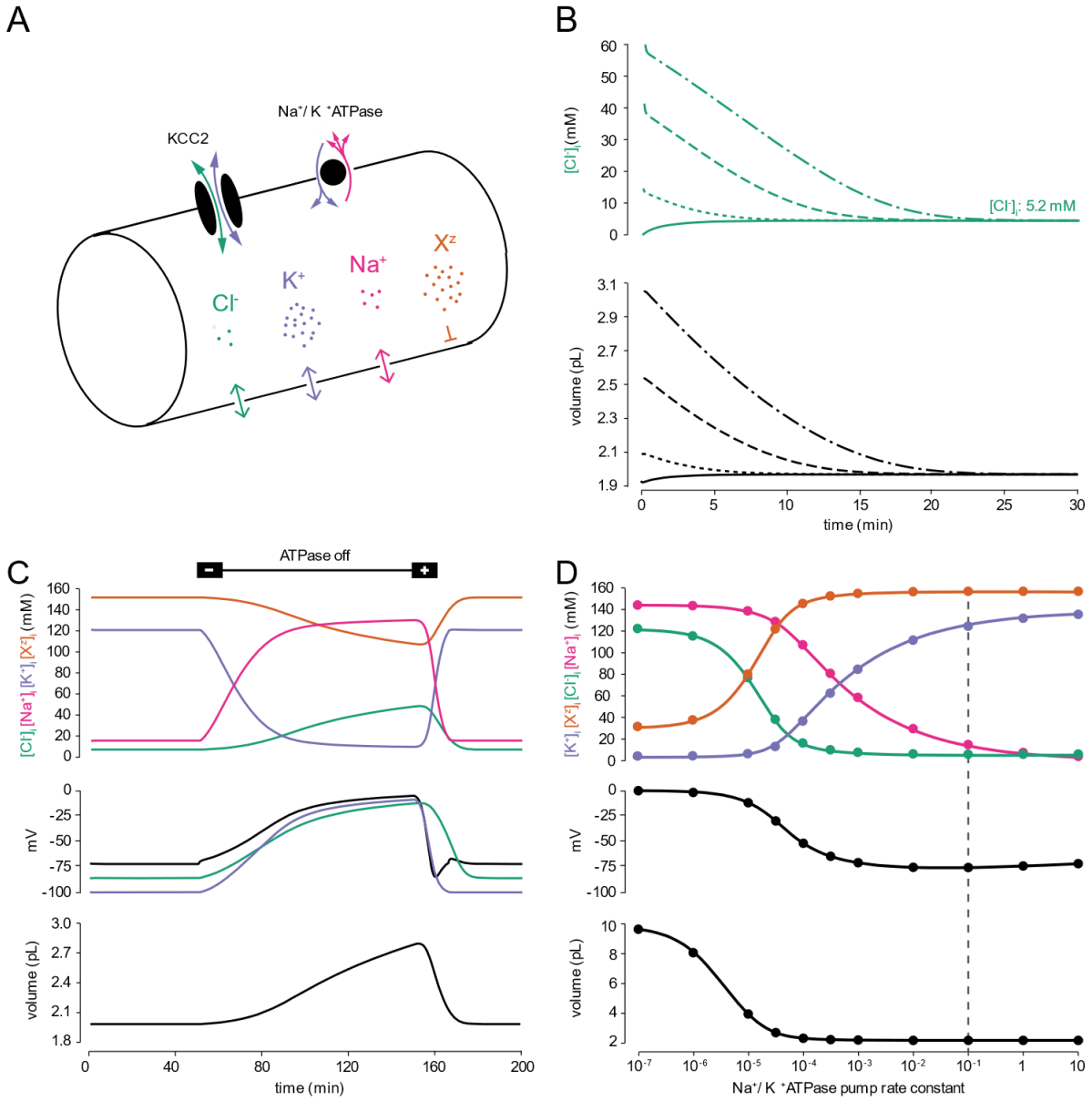

<u>Figure 1: A biophysical model of ion dynamics based on the pump-leak mechanism demonstrates the importance of the sodium-potassium ATPase for setting transmembrane ion gradients including chloride.</u> (A) A single cell compartment was modelled as a cylinder with volume changes equivalent to changes in cylindrical radius. Dynamics of membrane permeable potassium (purple, K^+), sodium (pink, Na^+) and chloride (green, Cl^-) ions were included. Impermeant anions (orange, X^z) had an average intracellular charge z. The KCC2 transporter moved Cl^- and K^+ in equal parts according to the transmembrane gradient for the two ions. The sodium-potassium ATPase transported 3 Na^+ ions in for 2 K^+ ions moved into the cell. (B) Regardless of intracellular starting concentrations of the permeable ions, the model converged to identical steady state values for all parameters without needing to include any means for 'sensing' ion concentration, volume or voltage. We show the result for Cl^- as a time series of Cl^- concentration (top panel) and volume (bottom panel). (C) The ATPase plays a key role in maintaining steady state ion concentration, membrane voltage (V) and volume. Switching off the ATPase results in a continuous increase in cell volume (bottom panel), membrane depolarization (middle panel) and ion concentration dysregulation (top panel with colours per ion as in 'A'. All cellular parameters recovered when the ATPase was reactivated. (D) The model's analytic solution showed exact correspondence with steady state values generated by numerical, time series runs (dots) for varying ATPase pump rates. Steady state values for the concentrations of the ions with colours as in A

(top panel); V (middle panel) and volume (bottom panel). The dashed line indicates the default ATPase pump rate used in all simulations unless specified otherwise.

Consistent with previous results (Dierkes et al., 2006; Dijkstra et al., 2016; Xiao et al., 2002), 'turning off' the activity of the Na^+/K^+ ATPase in our model led to a progressive collapse of transmembrane ion gradients, progressive membrane depolarization and continuous and unstable cell swelling. Such effects could be reversed by reactivation of the pump (**Fig. 1c**). The relative activity of the Na^+/K^+ ATPase sets the final stable values for ion concentrations (of both permeable and impermeant ions), V and volume (**Fig. 1c**). When we increased the activity of the Na^+/K^+ ATPase in our model, the final steady-state concentration for K^+ increased, whilst Na^+ and Cl^- dropped to levels that approximate those observed in mature neurons (**Fig. 1d**). At the same time, the final, stable-state membrane potential and cell volume also decreased. Interestingly, as has been observed previously (Fraser and Huang, 2004), beyond a certain level, further increases in Na^+/K^+ ATPase activity have negligible effects on cell volume and transmembrane voltage. For subsequent analysis, we chose a 'default' effective pump rate for the Na^+/K^+ ATPase of approximately 1.0×10^{-2} C/(dm^2.s), i.e. 7 pA with a pump rate constant of 10^{-1} (dimensionless, equation (2)), and average intracellular impermeant anion charge (z) of -0.85 as extrapolated from reasonable cellular ionic concentrations and osmolarity (Lodish et al., 2009; Raimondo et al., 2015). This resulted in steady-state ion concentrations and membrane potentials that approximate those experimentally observed in mature neurons: Cl^- 5 mM; K^+ 123 mM; Na^+ 14 mM; X^z 155 mM; and a V of -72.6 mV (Diarra et al., 2001; Jiang and Haddad, 1991; Tyzio et al., 2008). We were able to corroborate the numerical solutions for final steady-state values by developing a parametric-analytic solution (see Supplementary Material). We observed exact correspondence between the numerical and analytic solutions within our model (**Fig. 1d**). In subsequent analyses, this novel analytic solution allowed us to rapidly explore a large parameter space to determine how various cellular attributes might affect Cl^- homeostasis.

<u>Membrane chloride conductance affects steady-state intracellular chloride concentration only in the presence of active cation-chloride cotransport.</u>

Using the analytic solution, we investigated how changes in baseline ion conductance for the major ions in our model (g_K, g_{Na} and g_{Cl}) affected Cl^- homeostasis. We calculated the steady-state values for the Cl^- reversal potential (E_{Cl}) and potassium reversal potential (E_K), resting membrane potential (V) and volume (w) whilst independently manipulating the conductance for each ion (**Fig. 2**). Increasing the baseline potassium conductance (g_K) resulted in E_{Cl}, E_K and V converging to similar steady-state values (**Fig. 2a**) without significantly affecting cell volume. In contrast, increasing the baseline sodium conductance (g_{Na}) beyond 2 mS/dm^2 resulted in a steady depolarization of E_{Cl}, E_K and V with accompanying cell swelling (**Fig. 2b**).

The effect of manipulating Cl^- conductance (g_{Cl}) depended on the activity of concurrent cation-chloride cotransport by KCC2 (**Fig. 2c**). In the presence of active KCC2 at very low values of g_{Cl}, the steady state Cl^- concentration is such that E_{Cl} equals E_K. This follows because in the absence of alternative Cl^- fluxes, KCC2 utilizes the transmembrane potassium gradient to transport Cl^- until E_{Cl} equals E_K. With increasing g_{Cl} however, E_{Cl} increases, moving away from E_K towards V, and at very high Cl^- conductances E_{Cl} and V approached similar values in our model. Without the activity of KCC2, g_{Cl} had no effect on steady state E_{Cl}, E_K, V or volume (**Fig. 2d**). In this instance E_{Cl} always equals V as the movement of Cl^- across the membrane is purely passive. Without the activity of KCC2, there can be no driving force for Cl^- flux at steady state ($V - E_{Cl} = 0$). Our model therefore behaved in a manner consistent with established theoretical predictions (Kaila et al., 2014).

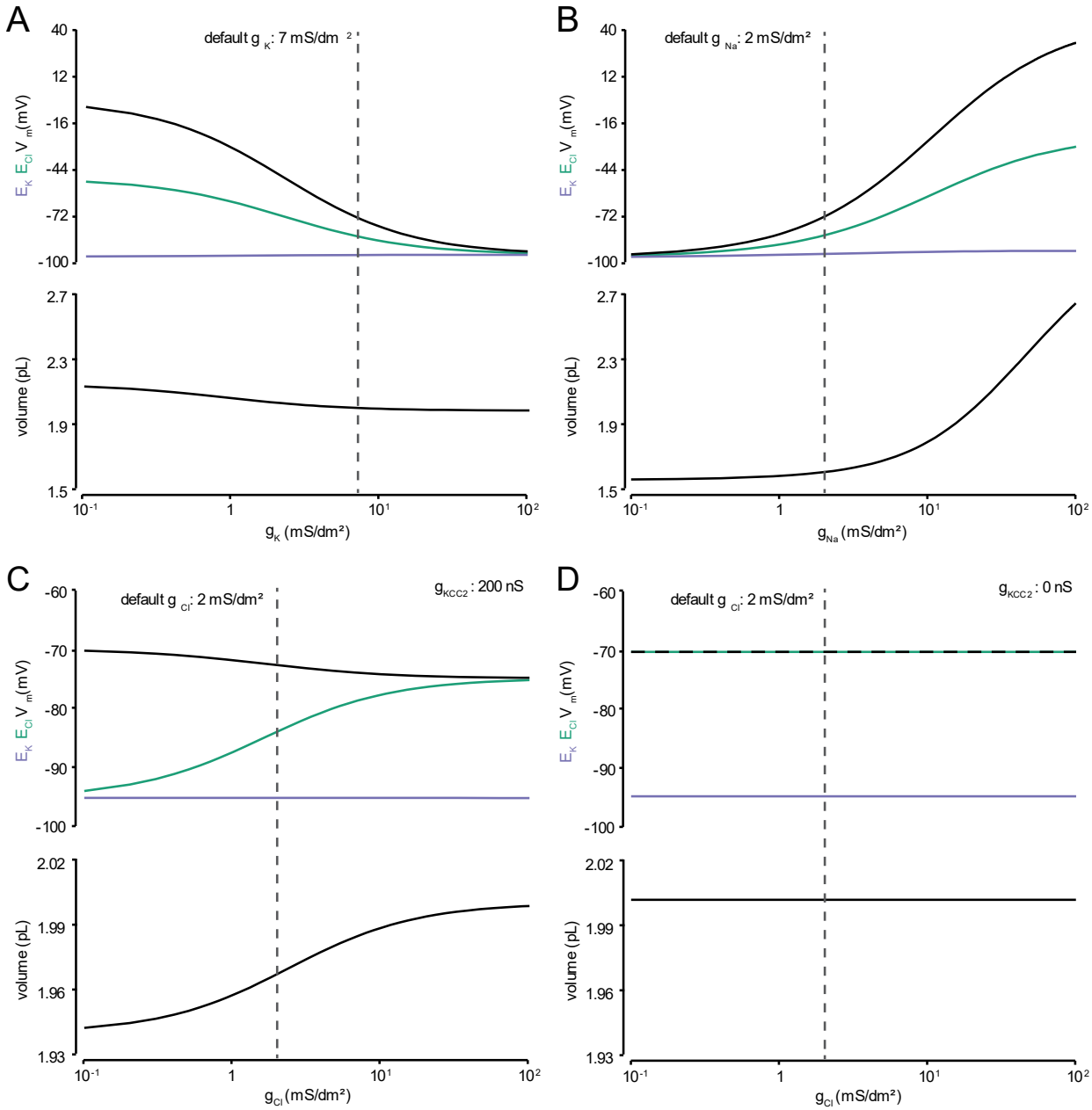

<u>Figure 2: Membrane chloride conductance affects steady-state intracellular chloride concentration only in the presence of active cation-chloride cotransport.</u> Steady state values for different ionic conductance were calculated using the model's analytic solution. (A) Steady state E_{Cl} (green), E_K (purple), V (black) and volume w (bottom panel) were calculated at different K^+ conductances (g_K). Increasing g_K resulted in a convergence of steady state E_{Cl}, E_K and V. (B) Increasing Na^+ conductance g_{Na} resulted in a progressive increase in steady state E_{Cl}, E_K and V with accompanying cell swelling. (C) In the presence of active cation-chloride cotransport (g_{KCC2} = 200 nS), increasing Cl^- conductance shifted steady state E_{Cl} from E_K toward V. (D) In the absence of KCC2 activity, g_{Cl} had no effect on steady state parameters. E_{Cl} equals V in all instances. Dashed lines indicate the default values for g_K, g_{Na} and g_{Cl}.

Cation-chloride cotransport sets the chloride reversal and driving force for transmembrane chloride flux.

Next, we used our single-cell unified model to explore how the activity of cation-chloride cotransport affects Cl^- homeostasis. In our model, the activity of KCC2 is set by the conductance of KCC2 (g_{KCC2}). Using the numerical formulation with the default values described in Figure 1 and 2, we steadily increased g_{KCC2} from 2 mS/dm^2 to 37 mS/dm^2 and tracked changes to E_{Cl}, E_K, V and volume. Increasing KCC2 activity over time caused a steady decrease in intracellular Cl^- concentration reflected by a hyperpolarization of E_{Cl} (**Fig. 3a**). V decreased only modestly, resulting in an increase in the driving force for Cl^- flux that tracks the increase in g_{KCC2}. This effect saturates as E_K constitutes a lower bound on E_{Cl}. Importantly, increases in g_{KCC2} resulted in persistent changes to E_{Cl} and the driving force for Cl^-. Using the analytic solution to our model we calculated how KCC2 activity affects steady state values of E_{Cl}, E_K, V, w and Cl^- driving force (**Fig. 3b**). In confirmation of our findings in Figure 2d, with no KCC2 activity ($g_{KCC2} = 0$), E_{Cl} equaled V and the Cl^- driving force was zero. As we increased g_{KCC2}, steady state E_{Cl} pulled away from V and approached E_K. This resulted in an increase in Cl^- driving force ($V-E_{Cl}$) with steady state values of 11.3 mV at our chosen default value of g_{KCC2}. The results obtained with our model are therefore fully consistent with the view that CCCs, in this case KCC2, establish the driving force for Cl^-.

To test this computational finding, we sought experimental data from the literature to determine whether changes in KCC2 activity correlate with alterations to steady-state intracellular Cl^- concentration. We focused on changes in KCC2 expression level, as this is likely to be a strong predictor of changes in KCC2 activity. Indeed, in a meta-analysis of 8 studies and 9 experiments from our review of 26 studies, weighted for methodological biases and data quality, we observed a correlation ($R^2 = 0.82$, $p < 0.001$) between change in KCC2 expression and intracellular Cl^- levels (**Fig. 3c**). This supports the prediction that cation-chloride cotransport by KCC2 is an important determinant of intracellular Cl^- concentration.

Since Cl^- cotransport by KCC2 depends on the transmembrane gradient for K^+, which in turn is established by the Na^+/K^+ ATPase, we explored how the Na^+/K^+ ATPase pump rate affected E_{Cl} in the presence of KCC2 activity ($g_{KCC2} = 2$ mS/dm^2). As depicted in **Fig. 3d**, the Na^+/K^+ ATPase pump is a critical determinant of intracellular Cl^- homeostasis. Of interest, above a pump rate constant of 10^{-3}, where cell volume is stable, even many fold changes in pump rate have minimal effects on E_{Cl} and V. It therefore seems unlikely that neurons would adjust the Na^+/K^+ ATPase to modulate Cl^- driving force.

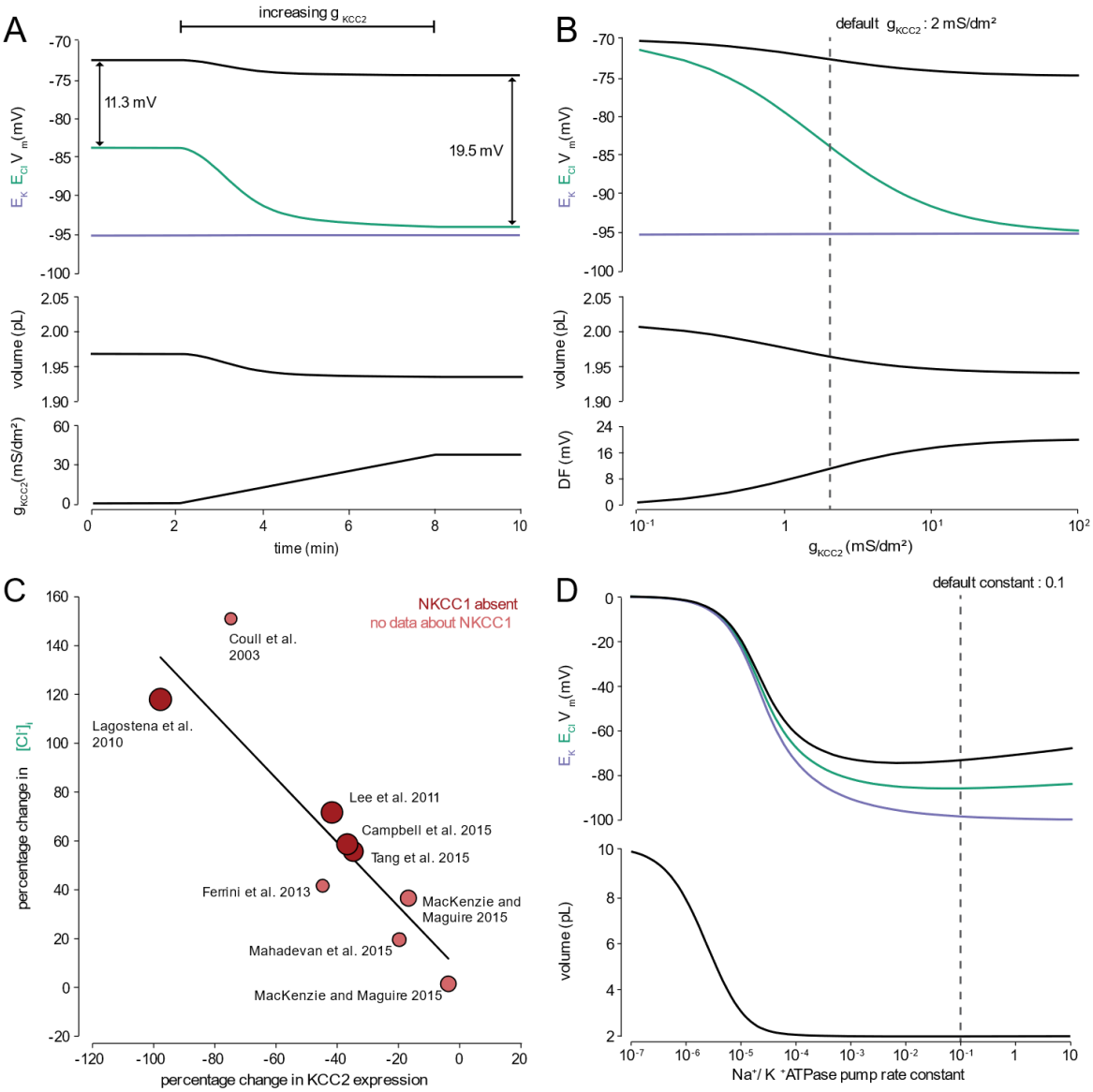

Figure 3: Cation-chloride cotransport sets the chloride reversal and driving force for transmembrane chloride flux. *(A) Increasing KCC2 activity in our model by increasing g_{KCC2} from 200 nS to 2 µS resulted in a persistent decrease in E_{Cl} (green), a minimal decrease in E_K (purple), V (black) and volume w (bottom panel). This resulted in a permanent increase in the driving force for Cl^- from -83.9 mV to -93.2 mV. (B) The steady state values for E_{Cl}, E_K, V (top panel), volume (middle panel) and Cl^- driving force (DF, bottom panel) at different KCC2 conductances. Increasing KCC2 activity resulted in a decrease in steady state E_{Cl} and chloride driving force. E_K represented a lower bound on E_{Cl} at high KCC2 conductances. (C) A meta-analysis of experimental studies demonstrates a correlation between KCC2 activity and intracellular Cl^- concentration confirming the role of KCC2 for establishing the neuronal Cl^- gradient in adult tissue. (D) Sufficient Na^+/K^+ ATPase activity critical for steady state ionic gradients, V (top panel, colours as in 'A') and volume (bottom panel), but these variables are relatively stable near the default pump rate (dashed line).*

Altering the concentration of intracellular or extracellular impermeant anions, without changing the average charge of impermeant anions, does not affect the steady state gradient or driving force for chloride.

To determine the effect of impermeant anions on Cl^- homeostasis we first explored whether adjusting the concentration of impermeant anions ($[X]_i$), while maintaining a constant average impermeant anion charge (z), had any impact on E_{Cl}, E_K, V or volume. We initiated the full single-compartment model with different starting concentrations of impermeant anions (but the same average charge, z = -0.85), and observed that regardless of the initial concentration of impermeant anions, over a period of minutes, the cell adjusted its volume to give an identical steady-state impermeant anion concentration (**Fig. 4a**, $[A]_i$ = 155 mM). Analytically, it can be shown that the number of moles of X determines completely the volume of the compartment, while the permeant ions alone cannot be used to predict steady state volume (Kay, 2017). Similarly, all initial impermeant anion concentrations resulted in identical steady state values of E_{Cl} (-83.8 mV), E_K (-95.1 mV) and V (-72.6 mV) (**Fig. 4b**). This shows that simply adjusting the amount of impermeant anions within a cell has no persistent effect on Cl^- concentration.

We then tested the effect of dynamically adding impermeant anions with the default average charge either intracellularly (**Fig. 4c**) or extracellularly (**Fig. 4d**). While impermeant anions are being added to the cell, the membrane potential hyperpolarizes and E_{Cl} decreases. However, following the cessation of impermeant anion influx, E_{Cl}, E_K, V and $[X]_i$ return to steady state values due to compensatory changes to cell volume (**Fig. 4c**). Impermeant ions (with default average charge) were added to the extracellular space, which is effectively an infinite bath in the model, while proportional decreases in $[Cl^-]_o$ were applied to correct for the changes to charge and osmotic balance. Additions in the extracellular space, similarly, resulted in a temporary depolarization of E_{Cl} and V, but no persistent shift in these parameters (**Fig. 4d**). The addition of extracellular impermeant anions did however result in a small compensatory decrease in cell volume secondary to the large shifts in Cl^- concentration required to maintain the proportion of $[Cl^-]_i$ to $[Cl^-]_o$ according to the Nernst potential. In summary, there is no lasting effect on the reversal potential or driving force for Cl^- if only the concentration of a neuron's intracellular or extracellular impermeant anions is altered.

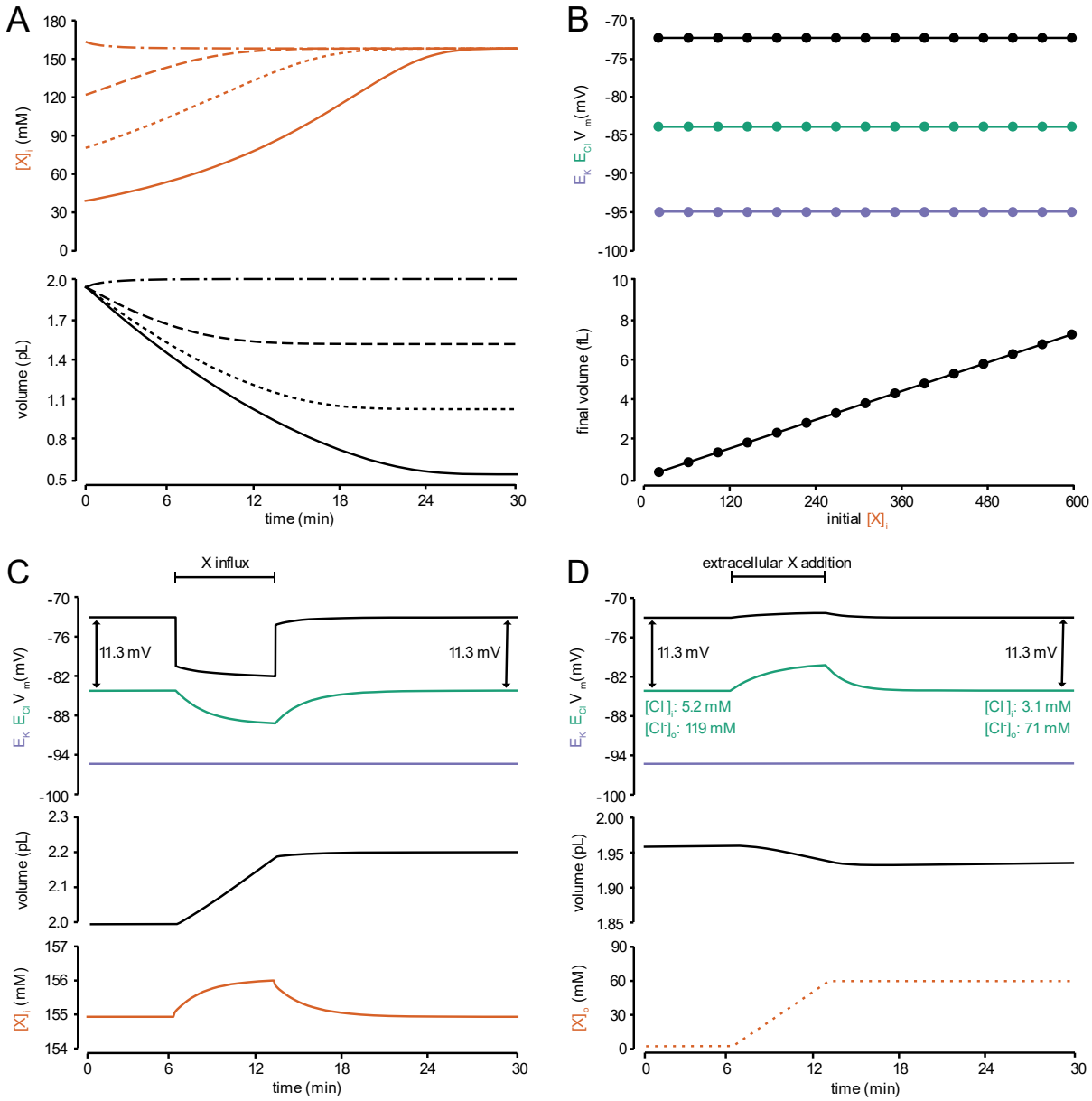

Figure 4: Adding intracellular or extracellular impermeant anions, without changing the average charge of impermeant anions, does not affect the steady state gradient or driving force for chloride. (A) Initiating the model with different starting concentrations of intracellular impermeant anions ($[X]_i$) with the same average charge z (orange, top panel), led to compensatory volume changes (bottom panel) which resulted in identical steady state concentrations. (B) Steady state E_{Cl} (green), E_K (purple) and V (black) were identical regardless of initial $[X]_i$. Final volume however was a linear function of initial $[X]_i$ (bottom panel). (C) Addition of impermeant anions of the same average charge (z) caused transients shifts in E_{Cl} (green, top panel), E_K (purple), V (black) as well as $[X]_i$ (orange, bottom panel) for the duration of the influx, and sustained increases in volume (black, middle panel). No persistent changes in E_{Cl}, E_K or V were observed. In contrast, a volume-constrained model including hydrostatic pressure was able to cause persistent changes in E_{Cl}, E_K or V, but not in the Cl^- driving force (dashed lines) (D) Similarly, the addition of extracellular impermeant anions in an osmoneutral manner and without affecting $[X]_i$ causes transient shifts in the permeable ion gradients (top panel, colours as in 'C'), and sustained changes in cellular volume (black, middle panel) as well as the extracellular X and extracellular and intracellular Cl^- concentrations.

Changing the average charge of impermeant anions can drive substantial shifts in the reversal potential for chloride, but has negligible effects on chloride driving force.

We next sought to determine how changes in the average charge of the impermeant ions (z) might influence the driving force on Cl^-. Such changes in average z, could be associated with various cellular processes, including post-translational modifications of proteins that decrease their charge without changing the absolute number of protein molecules, or pH changes where for example a carboxyl group is protonated. To investigate this parameter, we modified the average z of intracellular impermeant anions from -0.85 to -1 whilst measuring accompanying changes in E_{Cl}, E_K, V and cell (**Fig. 5a**). We found that this shift to a more negative average z resulted in both a transient and persistent decrease in E_{Cl}, E_K and V. Importantly, the shifts in E_{Cl} were accompanied by broadly matching shifts in E_K and V, which resulted in a small change in the driving force for Cl^- of < 0.2 mV. Both numerical and analytic calculation of steady state values for E_{Cl}, E_K and V in our model showed that changing the average charge of impermeant anions, while substantially affecting E_{Cl}, had very small effects on the driving force for Cl^- (**Fig. 5b**). By shifting z within reasonable ranges for mammalian neurons (Lodish et al., 2009; Raimondo et al., 2015), and assuming osmo- and electro-neutrality, only shifts of < 1 mV could be generated. In addition, although the absolute number of impermeant anions (moles) remained constant throughout the process of modifying z, cell volume shifted, and as a consequence modest alterations to the concentration of impermeant anions occurred as well.

Next, instead of adjusting the charge of existing anions in intracellular impermeant anions as described above, we directly added impermeant anions of differing valence to the cell (**Fig. 5c and d**). This had the effect of both increasing the absolute quantity of impermeant anions and adjusting the average charge of impermeant anions. The 'addition' of impermeant anions in this way models the *de novo* synthesis of impermeant anion species, or their active transport into the cell. This process also resulted in both transient and persistent changes to E_{Cl}, E_K and V, which was dependent on the extent that average z was altered. Again, whilst the large additions of impermeant anions could substantially alter the Cl^- reversal potential, this had a negligible effect on the driving force for Cl^- due to matching shifts in V. Importantly however, driving shifts in E_{Cl} in this manner resulted in large changes to cell volume (**Fig. 5d**). For example, a 3-fold increase in cell volume was observed when shifting z to -1.25 by adding impermeant anions of valence -1.5, yet this increase caused only a 5 mV change in E_{Cl}.

Our single compartment model of Cl^- homeostasis demonstrates that it is not the addition of impermeant anions *per se* but rather the adjustment of average impermeant anion charge that affects E_{Cl}. Interestingly, in the case in which z is changed, the driving force for Cl^- flux can be persistently altered, although only by very small amounts even for large shifts in z. This contrasts with the results shown earlier, where adjusting the activity of cation-chloride cotransport modulates both E_{Cl} and the driving force for Cl^- substantially.

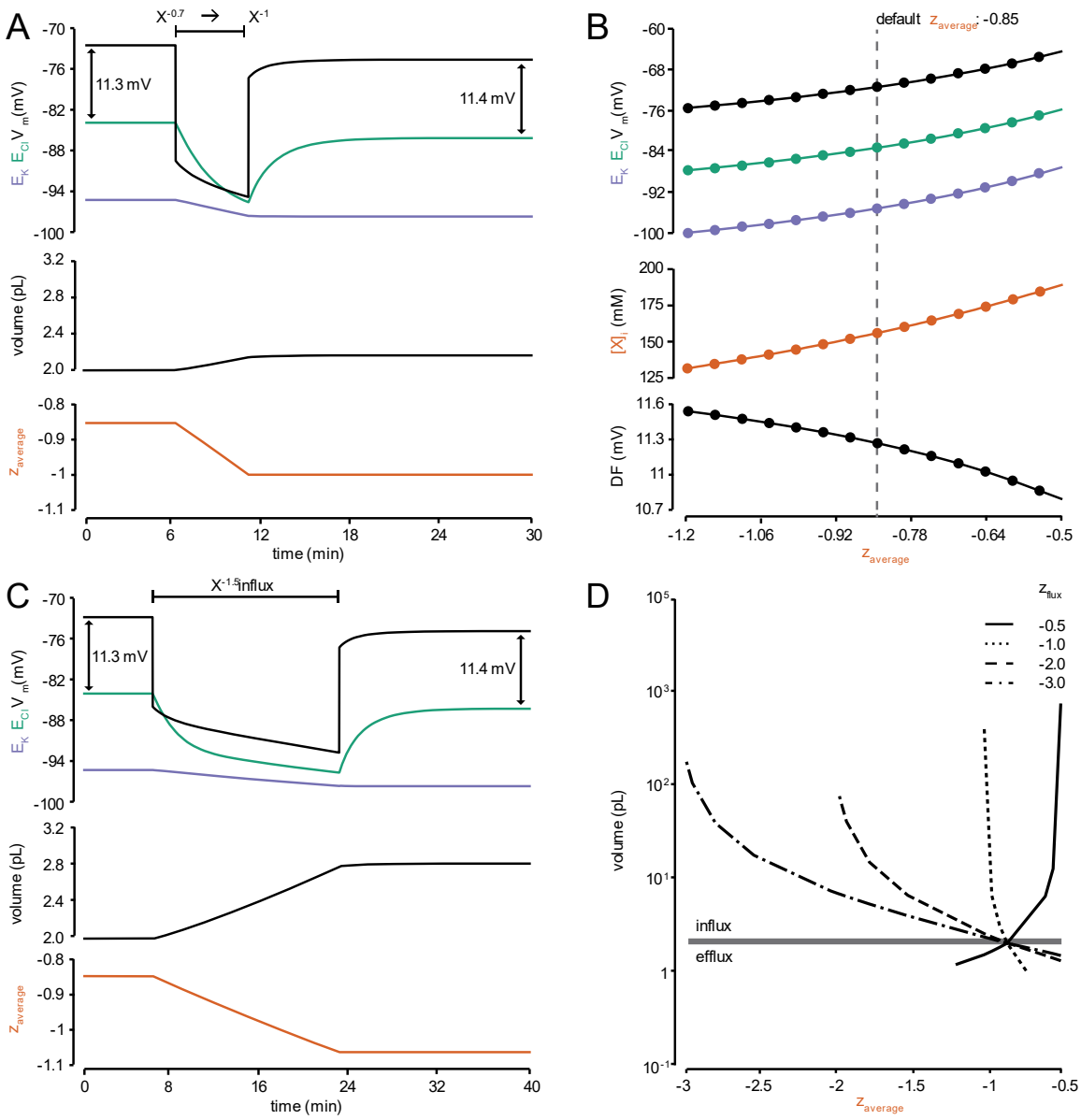

Figure 5: Adjusting the average charge of impermeant anions shifts the chloride reversal potential with negligible effects on the driving force for chloride. *(A) Decreasing the average charge of impermeant anions from -0.85 (the default value) to -1 (orange, bottom panel), without changing the absolute number of intracellular impermeant anions caused a persistent decrease in E_{Cl} (green, top panel), E_K (purple) and V with moderate increases in volume (middle panel) in our default single compartment model. Negligible changes in Cl^- driving force (0.16 mV) were observed. (B) The analytic solution (solid lines) for different impermeant anion average charge (z) exactly matches the steady state values from numerical, time series runs (dots) based on adjusting average z as in 'A'. Steady state E_{Cl}, E_K, V (top panel) and [X]i (middle) increased with increasing average z, while changes in average z resulted in no change in Cl^- driving force (bottom). The vertical dashed line indicates the values at the chosen default average z of -0.85. (C) Influx of a species of impermeant anions with average charge -1.5, that decreased average z (bottom panel) from -0.85 to -1 and increased the number of impermeant anions also caused persistent decreases of E_{Cl}, E_K and V as in 'A', but with much larger accompanying increases in cell volume (middle panel). Again, very small persistent changes in Cl^- driving force were observed. (D) Repeating the same change as in 'C' for species with different charges (z_{flux}) demonstrates the effect of driving shifts in the average intracellular impermeant charge on cell volume. Generating even small shifts in average z by adding or removing impermeant anions causes large changes in cell volume.*

371 Impermeant anions drive small shifts in chloride driving force by modifying the Na^+/K^+ ATPase pump
372 rate under conditions of active chloride cotransport.
373 We next set out to determine how, and under what conditions, the modification of impermeant
374 anions could generate the small persistent shifts in Cl^- driving force we observed. First, we repeated
375 the simulation performed in Figure 5a by changing the average charge of impermeant anions in the
376 cell, but under conditions where the Na^+/K^+ ATPase effective pump rate (J_p) was either a cubic function
377 of the transmembrane Na^+ gradient (default condition), or was fixed at a constant value (**Fig. 6a**). In
378 the case where the pump rate was fixed, adjusting the average charge of impermeant anions
379 generated no persistent change in Cl^- driving force (**Fig. 6a**). Modifying impermeant anions caused a
380 significant change in steady-state intracellular Na^+ concentration when J_p was kept constant. However,
381 small shifts in Cl^- driving force occurred only when the effective pump rate was variable, in which
382 minor changes to $[Na^+]_i$ caused significant changes to J_p, which in turn resulted in a small shift in Cl^-
383 driving force. There is a direct relationship between the average charge of impermeant anions (z),
384 $[Na^+]_i$, the effective Na^+/K^+ ATPase pump rate and Cl^- driving force. This relationship was abolished
385 when the effective Na^+/K^+ ATPase pump rate was held constant by removing its dependence on Na^+
386 (**Fig. 6b**). In addition, even large variations in effective pump rate near the default value caused
387 negligible shifts in Cl^- driving force of < 1 mV. These small, impermeant anion driven, Na^+/K^+ ATPase
388 pump dependent shifts in Cl^- driving force are completely dependent on the presence of cation-
389 chloride cotransport. In the absence of KCC2, there is no Cl^- driving force as E_{Cl} = V (**Fig. 6f**).
390
391 We then tested whether relaxing the condition of transmembrane osmoneutrality might also alter
392 impermeant anion induced effects on Cl^- driving force. We modelled a situation where increases in
393 cell surface area beyond a certain 'resting' surface area generated a hydrostatic pressure (membrane
394 tension), which could balance an osmotic pressure difference of 10 mM between the intra and
395 extracellular compartments (see **Fig. 6c**, schematic in **Fig. 6e** and Materials and Methods). In this case,
396 adding impermeant anions of default charge z resulted in constrained increases in cell volume, which
397 were accompanied by persistent transmembrane differences in osmolarity and intracellular Na^+
398 concentration. This was sufficient to generate small differences in driving force for Cl^- of < 0.2 mV for
399 reasonable increases in cell surface area (Dai et al., 1998; Nichol and Hutter, 1996). Again, this was
400 entirely due to Na^+ driven shifts in the Na^+/K^+ ATPase effective pump rate. By removing the
401 dependence of Na^+/K^+ ATPase activity on Na^+ concentration, addition of impermeant anions no longer
402 generated persistent shifts in Cl^- driving force (**Fig. 6c**). We observed a direct relationship between
403 transmembrane osmotic gradient, $[Na^+]_i$, the effective Na^+/K^+ ATPase pump rate and Cl^- driving force.
404 This relationship was removed when the effective Na^+/K^+ ATPase pump rate was held constant, with
405 no changes in Cl^- driving force seen despite the generation of the same shift in osmoneutrality (**Fig.**
406 **6d**).
407
408 In summary, changes in Cl^- driving force generated by changing the ionic contributions to cellular
409 charge (by altering the average charge of impermeant anions) or osmoneutrality (by increasing the
410 contribution of hydrostatic pressure) are due to the alteration of the dynamics of active ion transport
411 mechanisms in the cell. However, these effects are negligible in magnitude and cannot contribute
412 significantly to setting physiologically observed Cl^- driving forces. It is worth reiterating that any non-
413 zero Cl^- driving force is entirely dependent on the presence of active Cl^- cotransport. In our model, in
414 the absence of KCC2, neither the Na^+/K^+ ATPase nor impermeable anions can shift Cl^- out of
415 equilibrium (**Fig. 6f**).
416

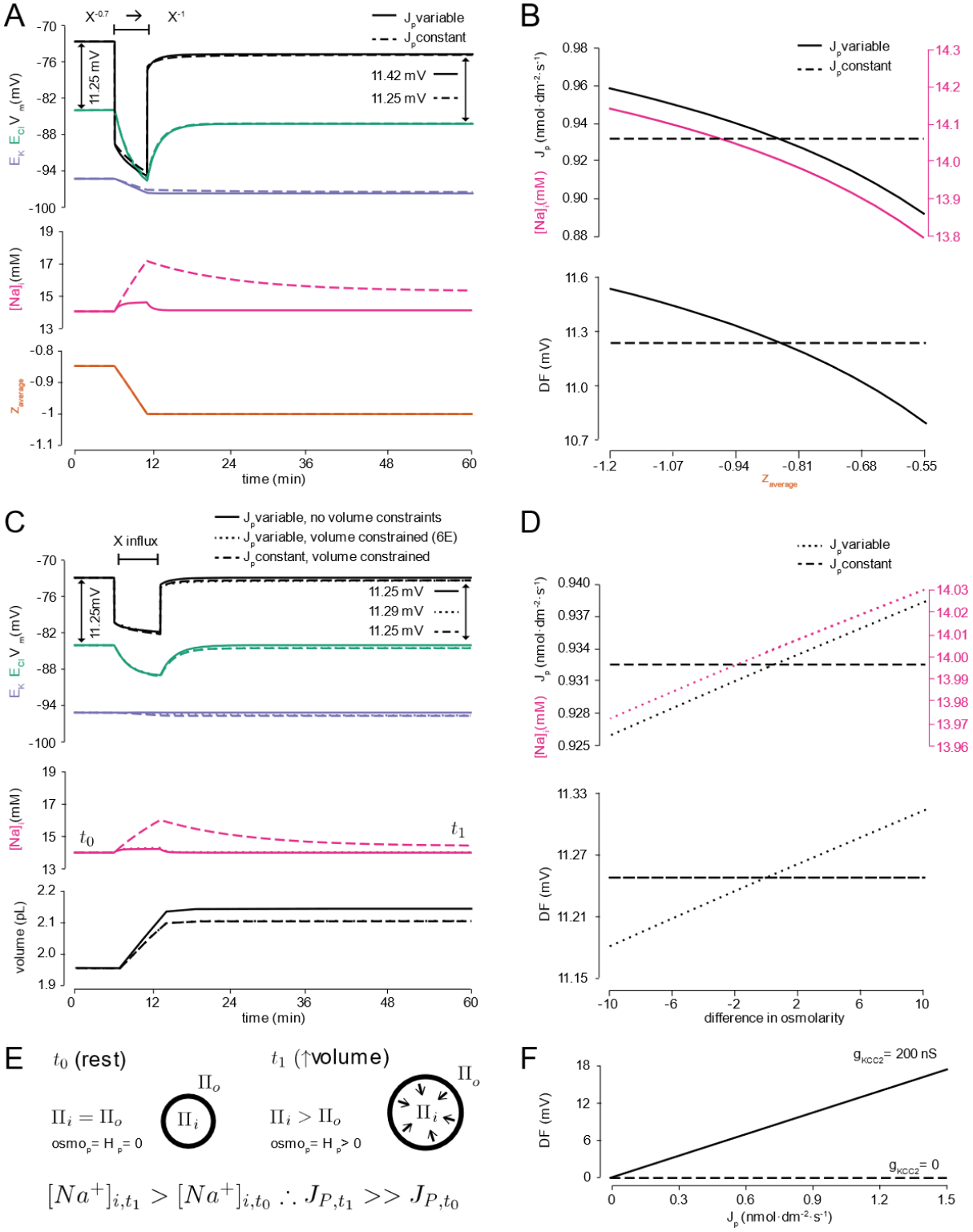

Figure 6: Impermeant anions drive small shifts in chloride driving force by modifying the Na^+/K^+ ATPase pump rate under conditions of active chloride cotransport. *(A) E_{Cl} (green), E_K (purple) and V (black) (top panel), $[Na^+]_i$ (pink, middle panel) and average impermeant anion charge z (orange, lower panel) over time in the default single compartment model. Changing the average z from -0.85 to -1 generated small, persistent Cl^- driving force shifts (arrows) only when the effective ATPase pump rate (J_p) was variable (solid line) and not when J_p was kept constant (dashed line). (B) Solving analytically across different values of z with either a variable J_p (solid lines) or a constant J_p (dashed line), demonstrates the direct relationship between Na^+ (pink), effective pump rate (J_p) (top panel) and Cl^- driving force (DF,*

lower panel). (C) E_{Cl} (green), E_K (purple) and V (black) (top panel), $[Na^+]_i$ (pink, middle panel) and cell volume (black, lower panel) over time in the default single compartment model. Impermeant anions of the same average charge of the cell were added (solid lines). A volume constraint was incorporated by adding a hydrostatic force dependent on membrane tension (dashed lines), which resulted in an impermeable anion induced transmembrane osmotic differential. This caused a small change in Cl^- driving force when J_p was variable (dashed line), but not when J_p was held constant (dotted lines). (D) Solving analytically across osmolarity differences demonstrates the direct relationship between Na^+ (pink), effective pump rate (J_p) (top panel) and Cl^- driving force (lower panel). Note, the small changes in Cl^- DF. (E) Schematic explaining the mechanism through which impermeant anion induced cell swelling in the presence of volume constraints (i.e. membrane tension) result in steady states with equal but non-zero osmotic ($osmo_P$) and hydrostatic pressures (H_P), causing transmembrane osmotic differences (t_1). This causes small changes in Na^+, and hence J_p. (F) All Na^+/K^+ ATPase pump rate-related shifts in the Cl^- driving force require KCC2 activity; in the absence of activity (dashes), no shifts in driving force can occur.

<u>Changes in cation-chloride cotransport activity generate local differences in chloride reversal and driving force, which depend on cytoplasmic diffusion rates.</u>

An important functional question is how Cl^- driving force might be modified at a local level within a neuron. We considered local persistent changes of Cl^- driving force for the case of active transmembrane Cl^- fluxes (**Fig. 7**) and impermeant anions (**Fig. 8**) by extending the single compartment model described above into a multi-compartment model or 'virtual dendrite.' This dendrite was 100 µm in length and consisted of ten compartments, each of 10 µm length and 1 µm diameter. The compartments contained the same mechanisms and default parameterization as the single compartment model described above. Compartmental volume was changed by altering the radius, while holding the length constant. In addition, all ions, except impermeant anions, could move between compartments by electrodiffusion (**Fig. 7a** and Materials and Methods).

To explore the local effects of CCC activity, we increased g_{KCC2} from our default value of 2 mS/dm^2 to 60 mS/dm^2 in the second last compartment of the virtual dendrite exclusively. This resulted in a persistent decrease in E_{Cl}, concurrent with a modest decrease in V, resulting in a permanent increase in Cl^- driving force and minimal change in compartment volume (**Fig. 7b**). The spatial precision of this alteration depended strongly on the diffusion constant for Cl^-. With a Cl^- diffusion constant of 2.03×10^{-7} dm^2.s^{-1}, these alterations spread widely through the virtual dendrite. For example, the change in Cl^- driving force was 4.8 mV in the furthermost compartment (90 µm apart) as compared to 5.9 mV in the compartment manipulated. When we decreased the Cl^- diffusion constant by one order of magnitude, the change in Cl^- driving force was 7.3 mV in the compartment in which KCC2 was adjusted, but only 1.8 mV in the furthermost compartment from the site of manipulation (**Fig. 7c**). These findings suggest that local differences in cation-chloride cotransport activity can drive spatially restricted differences in Cl^- driving force under conditions of constrained Cl^- diffusion, however under conditions of typical ionic diffusion the effect of Cl^- transport by KCC2 is widespread.

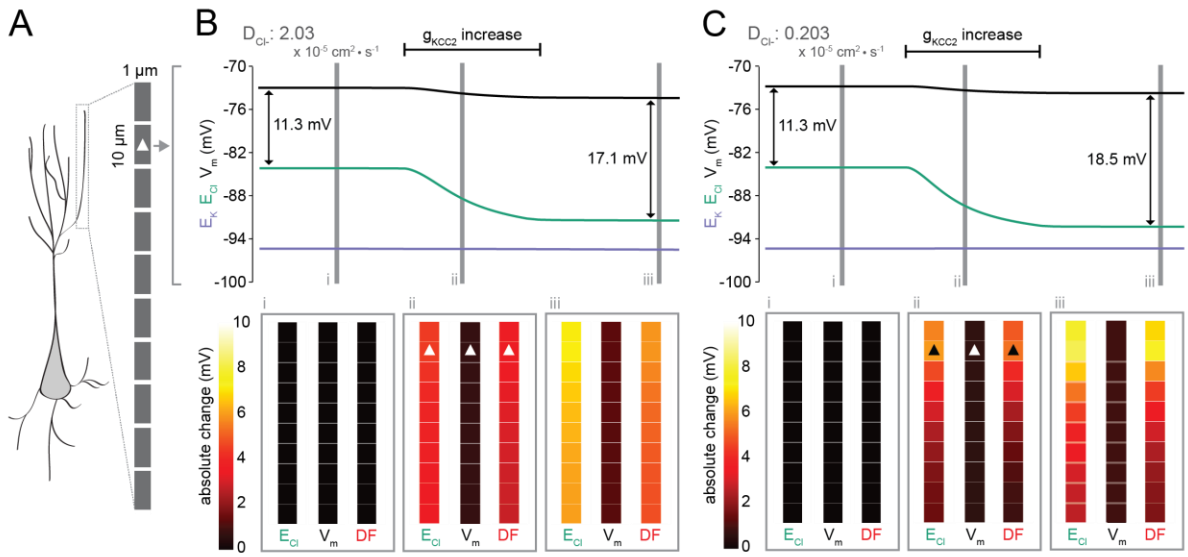

Figure 7: Local changes in KCC2 activity generate local differences in chloride reversal and driving force only under conditions of constrained chloride diffusion. (A) Schematic depicting the multi-compartment model representing a virtual dendrite of length 100 µm and radius 0.5 µm. The virtual dendrite consists of 10 compartments of initial length 10 µm. Each compartment contains the same mechanisms and default parameterization as the single compartment model. All ions, except impermeant anions, could move between compartments by electrodiffusion. (B) Top panel, E_{Cl} (green), E_K (purple) and V (black) from the 2nd from top compartment (indicated with a Δ) where the conductance of KCC2 was increased. The insets depict the length, and absolute change from baseline of E_{Cl}, V and DF for all compartments before (i), during (ii) and after (iii) the activity of KCC2 was selectively increased. This resulted in E_{Cl} decreasing in all compartments with minimal changes to E_K and V. Consequently, the driving force for Cl^- (DF) increased. In this case the diffusion constant for Cl^- (D_{Cl} = 2.03x10^{-7} dm^2.s^{-1}) resulted in E_{Cl} and DF changes being widespread across the virtual dendrite. (B) Reducing the Cl^- diffusion constant to 0.2x10^{-7} dm^2.s^{-1} resulted in a localized effect of compartment specific KCC2 activity increases on E_{Cl} and DF.

Local impermeant anions do not appreciably affect the local driving force for chloride.

Following the last result, we considered whether changing impermeant anions in part of a dendrite could create a local area with a different Cl^- driving force compared to the rest of the cell. We first added impermeant anions of average charge (z) exclusively to the second-last compartment of the virtual dendrite while measuring the Cl^- reversal, V and Cl^- driving force (DF) in all compartments. During addition of the impermeant anions, E_{Cl} and V decreased with an accompanying decrease in Cl^- driving force. However, following cessation of impermeant anion influx, all parameters returned to baseline levels, except for the volume of that specific compartment, which showed a modest increase (**Fig. 8b**). This suggests that local addition of impermeant anions of average charge has no local effect on Cl^- homeostasis but can affect the volume of the compartment concerned.

Next, we again added impermeant anions to the second-last compartment of the virtual dendrite, but this time we added impermeant anions with a more negative charge than average (z = -1). This resulted in the average charge of impermeant anions in that specific compartment becoming more negative (**Fig. 8c**). During the addition of the impermeant anions, E_{Cl} and V decreased across the dendrite, but with small accompanying shifts in Cl^- driving force. Following cessation of local impermeant anion influx, a persistent shift in E_{Cl} and V was observed specifically in the compartment manipulated. However, this generated a negligible, persistent change in Cl^- driving force (< 0.01 mV change in driving force for a compartment specific change in z from -0.85 to -0.93), and only within that specific compartment of the virtual dendrite. Again, impermeant anion addition resulted in a

permanent increase in the volume of the compartment concerned. This finding suggests that local impermeant anions can adjust the Cl^- reversal potential locally, but are not well-placed to cause significant, permanent shifts in the driving force for Cl^-. Indeed, electrodiffusion may further limit the degree to which changes in impermeant ion charge can modify driving forces through alterations in active ionic transport: the resulting permanent Cl^- driving force changes in the multi-compartment model are many times smaller than the shifts in the single compartment version (as compared to **Fig. 6b**).

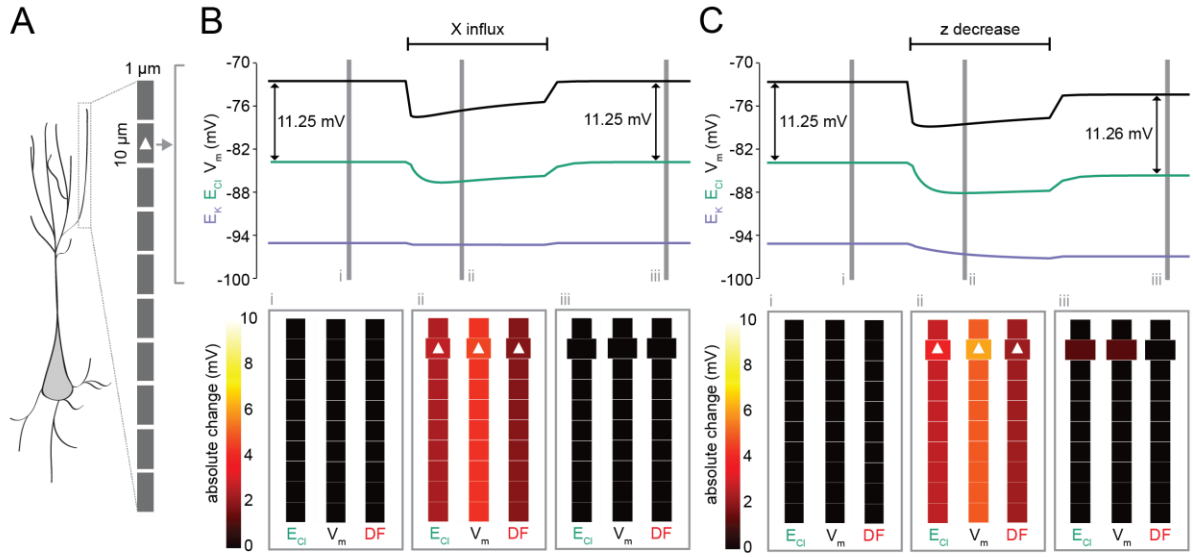

<u>Figure 8: Local changes in impermeant anions do not establish the local driving force for chloride.</u> (A) Multi-compartment model of a 10 compartment 100 µm virtual dendrite as in Figure 6. (B) Top panel, E_{Cl} (green), E_K (purple) and V (black) within the compartment where additional impermeant anions were exclusively added (indicated with a Δ). The insets depict the length, and absolute change from baseline for E_{Cl}, V and DF for each compartment of the virtual dendrite before (i), during (ii) and after (iii) impermeant anions were added (colour map as in 'A'). The selective addition of impermeant anions of average z selectively to the 2nd from top compartment only (arrow), resulted in transient but not permanent shifts in E_{Cl}, V and the Cl^- driving force (DF) in all compartments. The total length of the dendrite increased permanently due to an increase in the length of the compartment where impermeant anion addition occurred. (C) Traces and insets as in 'B' showing the addition of impermeant anions of different charge in order to decrease average z in the 2nd from top compartment specifically. Note that during addition of impermeant anions, E_{Cl}, E_K and V decreased across the dendrite but no change in DF was observed. A local persistent change in E_{Cl} and V was seen in the compartment manipulated (indicated with a Δ), which did not result in any permanent change in driving force for Cl^-. Again, impermeant anion addition resulted in a lengthening of the virtual dendrite.

Discussion

The driving force for Cl^- is a fundamental parameter affecting the excitability of neuronal networks (Raimondo et al., 2017). Computational models, which account for the dynamics of Cl^- ions, have been particularly useful in determining how transmembrane fluxes of Cl^- modulate inhibitory signaling in the brain (Lewin et al., 2012; Qian and Sejnowski, 1990; Staley and Proctor, 1999). These have demonstrated how dynamic changes to the driving force for Cl^- are critical for controlling the effect of synaptic inhibition (Doyon et al., 2011; Jedlicka et al., 2011; Lewin et al., 2012; Mohapatra et al., 2016). For example, dynamic Cl^- accumulation can degrade neural coding (Doyon et al., 2015) and contribute to the development and evolution of seizures (Krishnan and Bazhenov, 2011; Raimondo et al., 2015). Whilst previous models have included the Na^+/K^+ ATPase, the interacting dynamics of several ion species, CCCs (Doyon et al., 2011; Krishnan and Bazhenov, 2011), electrodiffusion (Qian and Sejnowski, 1989) and more recently impermeant anions and volume regulation (Dijkstra et al., 2016), none have combined all of these mechanisms to specifically explore how their combination determines the local driving force for Cl^-. Here we have explored the determinants of the Cl^- driving force in neurons by combining all of these mechanisms to generate a biophysically plausible model of Cl^- homeostasis. Using both numerical simulations and a novel analytic solution, we show that the Na^+/K^+ ATPase, baseline K^+, Na^+ and Cl^- conductances, average charge on impermeant anions, water permeability and CCCs all play a role in setting the Cl^- concentration within neurons. Importantly, we show that impermeant anions cannot alter the Cl^- driving force significantly under physiologically relevant conditions and as such represent an unlikely cellular strategy for modifying the properties of synaptic inhibition in the nervous system.

Experimentally elucidating the determinants of Cl^- driving force in the nervous system is challenging due to the existence of multiple dynamically interacting variables. In addition, while several techniques exist for measuring intracellular Cl^- concentration and V, many have significant drawbacks. For example, gramicidin perforated patch-clamp experiments, whilst allowing estimates of Cl^- indirectly via concurrent activation of Cl^- channels, perturb K^+ concentration and could erroneously estimate V (Tyzio et al., 2003). Genetically encoded reporters of Cl^-, whilst measuring Cl^- concentration directly, are intrinsically sensitive to pH, vulnerable to experimental artefact and importantly do not afford simultaneous read-out of V (Arosio and Ratto, 2014; Kuner and Augustine, 2000; Luhmann et al., 2014; Raimondo et al., 2013). The cell-attached approach using NMDA and $GABA_AR$ channel conductance to measure the driving force across $GABA_ARs$ may be minimally invasive, but cannot be used to explore local variations in Cl^- driving force (Tyzio et al., 2008). In light of these experimental challenges, the use of biophysically plausible computational models, based on theoretical 'first principles', represents a valuable strategy for exploring the potential determinants of Cl^- driving force in the nervous system.

Our approach is firmly based on the pump-leak formulation, first introduced by Tosteson and Hoffman (1960), which suggests that mammalian cells maintain their volume under the osmotic stress generated by the presence of impermeant anions and the Donnan effect by employing active transport of Na^+ and K^+ using the Na^+/K^+ ATPase (Armstrong, 2003; Kay, 2017). This maintains the cell volume by pumping ions across the membrane in a manner that stabilizes transmembrane osmotic differences. Neurons are never at a Donnan equilibrium as this is a true thermodynamic equilibrium, requiring no energy to maintain it. A Donnan equilibrium is not possible in cells with pliant membranes (Kay, 2017; Sperelakis, 2012). In contrast, the pump-leak mechanism sustains cells in a steady state, where ion concentration, voltage and volume are stable. It is a dynamic steady state that requires the continuous expenditure of energy to stabilize the cell.

Our model conforms to this framework in that abolishing the activity of the Na^+/K^+ ATPase leads to cell swelling and progressive membrane depolarization and rundown of ionic gradients. Importantly, as has been demonstrated before (Fraser and Huang, 2004), even two-orders of magnitude reductions

in physiological pump-rates at steady state result in negligible changes to cell volume (see **Fig. 1**). That is, cell volume is resistant to certain levels of Na^+/K^+ ATPase inhibition. This might explain recent experimental findings in which periods of Na^+/K^+ ATPase inhibition using ouabain caused modest changes to cell volume (Glykys et al., 2014). It is clear that the Na^+/K^+ ATPase is a fundamental cellular parameter that stabilizes cell volume and determines all ionic gradients including that of Cl^- and hence must be considered in any attempt to model ion homeostasis. Interestingly, we demonstrate that above a certain level of Na^+/K^+ ATPase activity, even many fold changes in pump rate have minimal effects on E_{Cl} and V. It therefore seems unlikely that neurons would adjust the Na^+/K^+ ATPase as a means for modulating Cl^- driving force specifically.

Baseline ion conductances are another important factor that affect Cl^- concentration and its driving force for membrane flux. Our model is consistent with recent experimental results that demonstrate that increased neuronal Na^+ conductance (for example by activating NMDA receptors, or preventing closure of voltage-gated Na^+ channels), leads to progressive neuronal swelling, membrane depolarization and Cl^- accumulation (Rungta et al., 2015) – the primary pathological process in cytotoxic oedema (Liang et al., 2007). This serves to confirm that the reduction of Na^+ permeability is fundamental to preventing the profligate use of energy in pump-leak mechanisms. It can be shown mathematically that the pump-leak mechanism will only generate a stable volume if $3[Na^+]_o/g_{Na}>2[K^+]_o/g_K$ (Keener and Sneyd, 1998). In addition, we show that the tonic neuronal Cl^- conductance only affects steady state Cl^- concentration and driving force in the presence of accompanying cation-chloride cotransport. Without active Cl^- flux of some kind, which CCCs provide, there is no driving force for passive Cl^- flux and hence no mechanism for Cl^- concentration changes resulting from selective modification of Cl^- conductance. This is consistent with both classic (Misgeld et al., 1986) and more recent experimental findings (Berglund et al., 2016). Using the sensor Clomeleon to image intracellular Cl^- in mouse cerebellum clearly demonstrates this phenomenon. That is, activation or blockade of tonic GABA conductances only modulate intracellular Cl^- concentration in the presence of functional cation-chloride cotransport (Berglund et al., 2016).

In the context of our model based on biophysical first principles, we find that increasing the activity of CCCs, in this case KCC2, increases the driving force for Cl^- flux by shifting the reversal potential for Cl^- closer to that of K^+. Interestingly, large shifts (~7 mV) in driving force were associated with very minor (1%) changes in volume or membrane potential. As such, we find that modulating KCC2 represents a specific means for manipulating the neuronal driving force for Cl^-. This is consistent with the traditional dogma in the field and previous experimental results (Kaila et al., 2014). In support of this view, our meta-analysis of experimental studies in adult rodent disease models showed a strong correlation between change in KCC2 expression and change in Cl^- concentration. Using our multi-compartment model, which incorporated electrodiffusion, we found that local modification of KCC2 activity has a specific local effect on Cl^- driving force depending on the characteristics of Cl^- diffusion (Mohapatra et al., 2016). In our model we needed to reduce cytoplasmic diffusion rates of Cl^- by an order of magnitude from current estimates in order to observe highly local Cl^- driving force changes driven by KCC2 (Kuner and Augustine, 2000; Qian and Sejnowski, 1989). Whilst differences in KCC2 activity might generate a gradient in Cl^- driving force between large subcellular structures (i.e. dendrites vs soma), our modelling results call into question the idea of synapse-specific Cl^- regulation within the same cellular domain (Földy et al., 2010). It is perhaps worth noting that the tortuosity of the intracellular environment could lead to decreases in the Cl^- diffusion coefficient (Verkman, 2002).

In this biophysical modelling study, we have performed the first extensive analysis of the possible means by which impermeant anions might affect Cl^- homeostasis. We find that modifying the number of impermeant anions inside or outside a neuron, without changing their average charge, has no persistent effect on intracellular Cl^- concentration, unless we include a cellular mechanism for allowing a transmembrane osmotic pressure differential to develop. This could include considering the cell

membrane as an elastic surface (like a balloon following Hooke's Law), which generates a hydrostatic pressure with increases in surface area. According to our model, where differences in intracellular and extracellular osmolarity on the order of 10 mM could develop due to membrane tension, shifts in Cl^- driving force of < 1 mV could occur. However, biological membranes lyse at even lower tensions than those generated by this range of oncotic pressures (Nichol and Hutter, 1996), so that an osmolarity difference of less than 5 mOsm is a more likely upper bound. Hence, impermeant anion driven shifts in transmembrane osmotic pressure differentials are unlikely to result in sizeable changes in Cl^- driving force.

Glykys et al. (2014) have provided some evidence that modifying the average charge of internal impermeant anions generates changes in local or cell-wide internal concentrations. This supports the idea that cellular differences in the average charge of anions, and/or transmembrane osmotic differences contribute to the wide variability of neuronal Cl^- concentrations observed experimentally (Glykys et al., 2014). However, we find that modifying the average charge of internal impermeant anions does not appreciably modify the driving force for Cl^-. This is because any impermeant anion driven change on intracellular Cl^- concentration and Cl^- reversal potential is matched by an equivalent effect on membrane potential V, resulting in negligible changes in the Cl^- driving force (Kaila et al., 2014; Voipio et al., 2014). However, given theoretical predictions (Kaila et al., 2014; Savtchenko et al., 2017; Voipio et al., 2014), it is interesting that changing impermeant anions could persistently affect the Cl^- driving force at all. We found that the small (< 1 mV) impermeant anion driven changes in Cl^- driving force we observed were caused by indirect effects on steady state Na^+ concentration and hence Na^+/K^+ ATPase activity. The impermeant anion driven changes in Cl^- driving force are even smaller in the multi-compartment model (<0.1 mV), in which electrodiffusion allows local changes in Na^+ to dissipate. When delinking Na^+/K^+ ATPase activity from the transmembrane Na^+ gradient, we found that impermeant anions were unable to cause any persistent shifts in Cl^- driving force as predicted theoretically (Kaila et al., 2014; Savtchenko et al., 2017; Voipio et al., 2014). It is important to note that these small, impermeant anion-Na^+/K^+ ATPase driven shifts in Cl^- driving force are entirely dependent on the presence of cation-chloride cotransport in the form of KCC2 and would entail changes in energy use by the Na^+/K^+ ATPase – active transport mechanisms are required to drive changes in Cl^- homeostasis.

Impermeant anions are one of a host of important cellular attributes which underpin cellular ion homeostasis. However, our models, which are fully consistent with biophysical first principles, suggest that impermeant anions alone cannot shift Cl^- out of equilibrium across the neuronal membrane. It therefore follows that neurons are unlikely to modify synaptic inhibition by altering impermeant anion concentrations or charge. Firstly, doing so would modify the resting membrane potential with little effect on the Cl^- driving force; and secondly, manipulation of impermeant anions is associated with profound changes to cell or compartment volume. The volume shifts may however reflect an important possible cellular function of impermeant ion transport. That is, neurons could use the transport and tethering of impermeant ions to grow or modify the volume of specific neuronal compartments.

In summary, using a biophysical model of Cl^- homeostasis we have shown that multiple cellular attributes underpin the driving force for Cl^- in neurons. Our work reaffirms the central importance of CCC activity for modulating Cl^- driving force and hence the properties of inhibitory synaptic transmission in the nervous system. Our findings have relevance for guiding the development of therapeutic strategies for manipulating Cl^- driving force in the context of neurological diseases caused by Cl^- dysregulation in the brain.

Materials and methods

Single compartment model. The single compartment model consisted of a cylindrical semi-permeable membrane separating the extracellular solution from the intracellular milieu with variable volume (**Fig. 1a**). The extracellular ionic concentrations were assumed constant (**Table 1**). Permeable ions in the model were K^+, Na^+ and Cl^- with their usual charges, while impermeant anions X were assumed to be a heterogeneous group of impermeant chemical species with average intracellular charge z and extracellular charge -1. z was chosen on the basis of known resting intracellular ion concentrations (Lodish et al., 2009; Raimondo et al., 2015) and Π (see Supplementary Material). The model included ionic leak currents for the permeable ions, Na^+/K^+ ATPase transporters and a CCC, in this case the K^+-Cl^- cotransporter (KCC2). Cell volume (w) change was based on osmotic water flux and incorporated a membrane surface area scaling mechanism. An analytical solution to the model at steady state was derived (see Supplementary Material). The numerical model was initialised assuming conditions close to electroneutrality and an osmotic equilibrium between the intracellular and extracellular compartments. A forward Euler approach was used to update variables at each time step (dt) of 1 ms. Using a smaller dt did not influence the results in Figure 1-5. Code was written in Python 2.

Membrane potential. The membrane potential V was based on the "Charge Difference" approach of Fraser and Huang (2004) as follows:

$$V = \frac{F\,([Na^+]_i + [K^+]_i - [Cl^-]_i + z[X^z]_i)}{C_m A_m} \tag{1}$$

where F is Faraday's constant, C_m is the unit membrane capacitance and A_m is calculated as the ratio of the surface area to cell volume. The term in brackets is the sum of all ionic charges within the cell. This approach has the advantage that the initial voltage can be calculated without needing to assume a steady state as is required for by the Goldman-Hodgkin-Katz (GHK) equation.

Permeable ion concentrations. Intracellular concentrations of the permeable ions Na^+, K^+ and Cl^- were updated individually by summing trans-membrane fluxes. Leak currents were calculated using the standard equivalent circuit formulation $I = g(V - E)$. In addition, Na^+ and K^+ were transported actively by the Na^+/K^+ ATPase, with pump rate J_p, which was approximated by a cubic function dependent on the transmembrane sodium gradient, following Keener and Sneyd (1998):

$$J_p = \frac{P}{F}\left(\frac{[Na^+]_i}{[Na^+]_o}\right)^3, \tag{2}$$

where P is the pump rate constant. Because it is a function of the sodium gradient, J_p decreases as $[Na^+]_i$ depletes. This formulation has been shown to be similar to more accurate kinetic models reliant on both the Na^+ gradient and ATP concentration (Keener and Sneyd, 1998). To switch the ATPase pump on or off (**Fig. 1c**), P was decreased/increased exponentially over 10-20 minutes, consistent with previous reports of the dynamics of inhibition of the ATPase by ouabain and in turn the inhibition of ouabain's effects by potassium canrenoate (Baker and Willis, 1972; Yeh and Lazzara, 1973). The ATPase pumps 2 K^+ ions into the cell for every 3 Na^+ ions out and these constants must be multiplied by J_p for each ion respectively. K^+ and Cl^- were influenced by flux through the type 2 K-Cl cotransporter (KCC2), J_{KCC2} (Doyon et al., 2016):

$$J_{KCC2} = g_{KCC2}(E_K - E_{Cl}), \tag{3}$$

where g_{KCC2} is a fixed conductance and E_K and E_{Cl} are the Nernst potentials for K^+ and Cl^- respectively. J_{KCC2} is 0 when E_K=E_{Cl}. The rate of change of the intracellular concentration of the three permeant ions was given by the following equations, with the Nernst potentials for each ion given by $E_{ion} =$

$\frac{RT}{zF}\ln\left(\frac{[ion]_{out}}{[ion]_{in}}\right)$, w indicating the cell volume, and $\frac{dw}{dt}$ as described in equation (7) (**Fig. 1-5, 6a, b, 7 and 8**) or (9) (**Fig. 6c-e**):

$$\frac{d[Na^+]_i}{dt} = -\frac{A_m}{F}\left(g_{Na}(V_m - E_{Na}) + 3J_p\right) - \frac{1}{w}\frac{dw}{dt}[Na^+]_i \tag{4}$$

$$\frac{d[\mathrm{K}^+]_i}{dt} = -\frac{A_m}{F}\left(g_K(V_m - E_K) - 2J_p - J_{KCC2}\right) - \frac{1}{w}\frac{dw}{dt}[K^+]_i \tag{5}$$

$$\frac{d[\mathrm{Cl}^-]_i}{dt} = \frac{A_m}{F}\left(g_{Cl}(V_m - E_{Cl}) + J_{KCC2}\right) - \frac{1}{w}\frac{dw}{dt}[Cl^-]_i. \tag{6}$$

Volume. Because the osmotic flux of water is expected to be faster than ion fluxes, the volume of the cell was adjusted to preserve transmembrane osmotic balance at each time step. Change in compartment volume, w, was calculated by changing the previous volume proportional to the difference between intracellular and extracellular osmolarity, Π_i and Π_o respectively (Hernández and Cristina, 1998), where v_w is the partial molar volume of water, p_w the osmotic permeability of a biological membrane and SA the surface area:

$$\frac{dw}{dt} = v_w \cdot p_w \cdot SA \cdot (\Pi_i - \Pi_o). \tag{7}$$

For the experiment in Figure 6c-e, where we allowed transmembrane differences in osmolarity to develop, we assumed that at rest the cylindrical cell had a radius of r_a and zero pressure across the membrane, and that the tension (T) in the membrane followed Hooke's law such that the tension was proportional to the difference between the dynamic circumference of the cell and that of the resting state. From Laplace's law the hydrostatic pressure in the cell was given by:

$$H_p = \begin{cases} 4\pi k_m\left(1 - \frac{r_a}{r}\right) & r > r_a \\ 0 & , \ otherwise \end{cases} \tag{8}$$

where k_m is the spring constant of the membrane (Sachs and Sivaselvan, 2015). Equation (7) was thus reformulated:

$$\frac{dw}{dt} = v_w \cdot p_w \cdot SA \cdot \left(\Pi_i - \Pi_o - \frac{H_p}{RT}\right). \tag{9}$$

In order to simulate extreme conditions of constrained volume, a larger k_m was employed than is realistic (Dai et al., 1998). Intracellular ion concentrations were updated again after volume change at each time step. Volume changes were manifested in the cylindrical compartment as change in the radius. In Figure 1-6, the cell was initialised with diameter 10 µm and length 25 µm.

Anion flux. Impermeant anions were manipulated in the compartment in Figure 4-6 and Figure 8 through several mechanisms. Anions could be added to the compartment at a constant rate dependent on A_m and have either the same average intracellular X charge z = -0.85 (**Fig. 4c, 6c and 8b**), or a different charge (**Fig. 5c, d, 6a and 8c**). In these cases, the number of moles of X in the compartment was increased. Alternatively, the charge of a species of intracellular X was slowly changed imitating a charge-carrying trans-membrane reaction (**Fig. 5a and 6a**). In this case, the

number of moles of intracellular X did not change and it was assumed charge imbalance was mopped up by the extracellular milieu. Finally, extracellular X^- was changed in Figure 4d by removing as much Cl^- as X^- was added, thus maintaining osmolarity and electroneutrality in the extracellular space.

Multi-compartment model. The single compartment dendrite model was incorporated in a multi-compartment model by allowing electrodiffusion to occur between individual compartments operating as described above. Compartments were initialised with a radius of 0.5 µm and length of 10 µm. Compartments were linked linearly without branching; a total length of 10 connected compartments was used. The time step dt was decreased to 10^{-3} ms for simulations in multiple compartments. Code was written in Python 3.

Electrodiffusion. The Nernst-Planck equation (NPE) was used to model one-dimensional electrodiffusion, based on Qian and Sejnowski (1989). The NPE incorporates fluxes because of diffusion and drift (i.e. the movement of ions driven by an electric field). It has been shown to be more accurate than using $J_{diffusion}$ alone in small structures like dendrites (Qian and Sejnowski, 1989). The NPE for J the flux density of ion C is calculated:

$$J = -D\frac{zF^2}{RT}[C]\frac{dV_m}{dx} - DF\frac{d[C]}{dx}, \tag{10}$$

where D is the diffusion constant of ion C (**Table 1**), z is its charge, [C] is its concentration and x is the distance along the longitudinal axis over which electrodiffusion occurs. The NPE was implemented between compartments i and i+1, assuming the i→i+1 direction was positive, using a forward Euler approach. The midpoints of the compartments were used to calculate dx, i.e. $dx = \frac{h_i + h_{i+1}}{2}$, and the concentrations of C in each compartment were averaged to obtain J_{drift}, ensuring that $J_{i\to i+1} = J_{i+1\to i}$, where the fluxes had units of mol/(s.dm^2):

$$J_{i\to i+1} = -D\left(\frac{zF}{RT}\frac{([C]_i + [C]_{i+1})}{2}\frac{dV_m}{dx} + \frac{d[C]}{dx}\right). \tag{11}$$

The flux was multiplied by the surface area between compartments and then divided by compartment volume to determine the flux in terms of molar concentration (M/s), i.e. $\frac{\pi r^2}{\pi r^2 h_i} = \frac{1}{h_i}$, and finally implemented numerically with a forward Euler approach. The implementation mirrored that in Qian and Sejnowski (1989) for non-branching dendrites, but was adjusted for compartments whose volumes can change:

$$C_{i\to i+1} = -\frac{dt}{h_i}D\left(\frac{zF}{RT}\frac{([C]_i + [C]_{i+1})}{2}\frac{(V_{m_i} - V_{m_{i+1}})}{dx} + \frac{([C]_i - [C]_{i+1})}{dx}\right). \tag{12}$$

	Value	Description
Constants		
F	96485.33 C/mol	Faraday constant
R	8.31446 C/V	Universal gas constant
T	310.15 K	Absolute temperature (=37°C)
Parameters		
C_m	2×10^{-4} F/dm^2	Unit membrane capacitance

g_{Na}	2×10^{-3} S/dm^2	Na^+ leak conductance
g_K	7×10^{-3} S/dm^2	K^+ leak conductance
g_{Cl}	2×10^{-3} S/dm^2	Cl^- leak conductance
g_{KCC2}	2×10^{-3} S/dm^2	KCC2 conductance
v_w	0.018 dm^3/mol	Partial molar volume of water
p_w	0.0015 dm.s	Osmotic permeability
k_m	25 N/dm	Variable for membrane tension (higher than reported: used in this paper to accentuate differences in osmolarity)
p	0.1 C/(dm^2.s)	Default pump rate constant
$[Na^+]_o$	145 mM	Extracellular Na^+ concentration
$[K^+]_o$	3.5 mM	Extracellular K^+ concentration
$[Cl^-]_o$	119 mM	Extracellular Cl^- concentration
$[X^-]_o$	29.5 mM	Extracellular impermeant anion (X) concentration
D_{Na}	1.33×10^{-7} dm^2/s	Na^+ diffusion constant
D_K	1.96×10^{-7} dm^2/s	K^+ diffusion constant
D_{Cl}	2.03×10^{-7} dm^2/s	Cl^- diffusion constant
Variables (default steady state)		
V	-72.6 mV	Membrane potential
$[Na^+]_i$	14.0 mM	Intracellular Na^+ concentration
$[K^+]_i$	122.9 mM	Intracellular K^+ concentration
$[Cl^-]_i$	5.2 mM	Intracellular Cl^- concentration
$[X^z]_i$	154.9 mM	Intracellular impermeant anion (X) concentration
z	-0.85	Average charge of intracellular X
w	2.0 pL (single compartment) 0.078 pL (multi-compartment)	Volume

Table 1: Constants, default parameters and usual steady state values for variables used in the biophysical model.

Systematic review. A literature search was performed to identify experimental studies that aimed to correlate a change in KCC2 expression with changes in $[Cl^-]_i$. The MEDLINE database was used and accessed via the PubMed online platform. Search terms included 'chloride', 'Cl', 'intracellular', 'KCC2', 'cotransporter', 'neuronal', 'GABA' using appropriate Boolean operators. Only studies that demonstrated changes in KCC2 expression and E_{GABA} were considered for the meta-analysis. As there is a well described differential expression of KCC2 and NKCC1 at different stages of development, only studies that used tissue older than postnatal day 7 were included; other exclusion criteria are shown in Figure S1 in Supplementary Material. Nine experiments from eight studies met all criteria and were included (Campbell et al., 2015; Coull et al., 2003; Ferrini et al., 2013; Lagostena et al., 2010; Lee et al., 2011; MacKenzie and Maguire, 2015; Mahadevan et al., 2015; Tang et al., 2015). To accommodate

810 varied experimental preparations and techniques influencing data quality and biases, a 34-point
811 scoring system was designed to weight the studies (see **Table S1** Supplementary Material). A weighted
812 least squares regression model was then used to correlate the percentage (%) change in KCC2
813 expression vs % change in $[Cl^-]_i$. Data used in regression can be seen in Table S2 (Supplementary
814 Material).
815
816 *References*
817

818 Ambros-Ingerson, J., and Holmes, W. R. (2005). Analysis and comparison of morphological
819 reconstructions of hippocampal field CA1 pyramidal cells. *Hippocampus* 15, 302–15.
820 doi:10.1002/hipo.20051.
821 Armstrong, C. M. (2003). The Na/K pump, Cl ion, and osmotic stabilization of cells. *Proc. Natl. Acad.*
822 *Sci. U. S. A.* 100, 6257–6262. doi:10.1073/pnas.0931278100.
823 Arosio, D., and Ratto, G. M. (2014). Twenty years of fluorescence imaging of intracellular chloride. 8,
824 1–12. doi:10.3389/fncel.2014.00258.
825 Baker, P. F., and Willis, J. S. (1972). Inhibition of the sodium pump in squid giant axons by cardiac
826 glycosides: dependence on extracellular ions and metabolism. *J. Physiol.* 224, 463–475.
827 Ben-Ari, Y. (2002). Excitatory actions of GABA during development: the nature of the nurture. *Nat.*
828 *Rev. Neurosci.* 3, 728–739. doi:10.1038/nrn920.
829 Berglund, K., Wen, L., Dunbar, R. L., Feng, G., and Augustine, G. J. (2016). Optogenetic Visualization of
830 Presynaptic Tonic Inhibition of Cerebellar Parallel Fibers. *J. Neurosci.* 36, 5709–5723.
831 doi:10.1523/JNEUROSCI.4366-15.2016.
832 Burton, R. F. (1983). The composition of animal cells: solutes contributing to osmotic pressure and
833 charge balance. *Comp. Biochem. Physiol.* 76B, 663–71.
834 Campbell, S. L., Robel, S., Cuddapah, V. A., Robert, S., Buckingham, S. C., Kahle, K. T., and Sontheimer,
835 H. (2015). GABAergic disinhibition and impaired KCC2 cotransporter activity underlie tumor-
836 associated epilepsy. *Glia* 63, 23–36. doi:10.1002/glia.22730.
837 Coull, J. A. M., Boudreau, D., Bachand, K., Prescott, S. A., Nault, F., Sík, A., De Koninck, P., and De
838 Koninck, Y. (2003). Trans-synaptic shift in anion gradient in spinal lamina I neurons as a
839 mechanism of neuropathic pain. *Nature* 424, 938–42. doi:10.1038/nature01868.
840 Dai, J., Sheetz, M. P., Wan, X., and Morris, C. E. (1998). Membrane Tension in Swelling and Shrinking
841 Molluscan Neurons. *J. Neurosci.* 18, 6681–6692.
842 Diarra, A., Sheldon, C., and Church, J. (2001). In situ calibration and [H+] sensitivity of the fluorescent
843 Na+ indicator SBFI. *Am. J. Physiol. Cell Physiol.* 280, C1623–C1633. doi:10.1016/S0165-
844 5876(00)00363-3.
845 Dierkes, P. W., Wüsten, H. J., Klees, G., Müller, A., and Hochstrate, P. (2006). Ionic mechanism of
846 ouabain-induced swelling of leech Retzius neurons. *Pflugers Arch. Eur. J. Physiol.* 452, 25–35.
847 doi:10.1007/s00424-005-0009-6.
848 Dijkstra, K., Hofmeijer, J., van Gils, S., and van Putten, M. J. A. M. (2016). A Biophysical Model for
849 Cytotoxic Cell Swelling. *J Neurosci* in press, 11881–11890. doi:10.1523/JNEUROSCI.1934-
850 16.2016.
851 Doyon, N., Prescott, S. a., Castonguay, A., Godin, A. G., Kröger, H., and De Koninck, Y. (2011). Efficacy
852 of Synaptic Inhibition Depends on Multiple, Dynamically Interacting Mechanisms Implicated in
853 Chloride Homeostasis. *PLoS Comput. Biol.* 7, e1002149. doi:10.1371/journal.pcbi.1002149.
854 Doyon, N., Prescott, S. A., and De Koninck, Y. (2015). Mild KCC2 hypofunction causes inconspicuous
855 chloride dysregulation that degrades neural coding. *Front. Cell. Neurosci.* 9, 1–16.
856 doi:10.3389/fncel.2015.00516.
857 Doyon, N., Vinay, L., Prescott, S. A., and De Koninck, Y. (2016). Chloride Regulation: A Dynamic
858 Equilibrium Crucial for Synaptic Inhibition. *Neuron* 89, 1157–1172.
859 doi:10.1016/j.neuron.2016.02.030.
860 Farrant, M., and Kaila, K. (2007). The cellular, molecular and ionic basis of $GABA_A$ receptor signalling.

Prog. Brain Res. 160, 59–87.
Ferrini, F., Trang, T., Mattioli, T. M., Laffray, S., Del'Guidice, T., Lorenzo, L., Castonguay, A., Doyon, N., Zhang, W., Godin, A. G., Mohr, D., Beggs, S., Vandal, K., Beaulieu, J., Cahill, C. M., Salter, M. W., and De Koninck, Y. (2013). Morphine hyperalgesia gated through microglia-mediated disruption of neuronal Cl− homeostasis. *Nat. Neurosci.* 16, 183–192. doi:10.1038/nn.3295.
Földy, C., Lee, S.-H., Morgan, R. J., and Soltesz, I. (2010). Regulation of fast-spiking basket cell synapses by the chloride channel ClC-2. *Nat. Neurosci.* 13, 1047–9. doi:10.1038/nn.2609.
Fraser, J. A., and Huang, C. L.-H. (2004). A quantitative analysis of cell volume and resting potential determination and regulation in excitable cells. *J. Physiol.* 559, 459–78. doi:10.1113/jphysiol.2004.065706.
Glykys, J., Dzhala, V., Egawa, K., and Balena, T. (2014). Local Impermeant Anions Establish the Neuronal Chloride Concentration. *Science 343*, 670–676. doi:10.1126/science.1245423.
Hernández, J. a, and Cristina, E. (1998). Modeling cell volume regulation in nonexcitable cells: the roles of the Na+ pump and of cotransport systems. *Am. J. Physiol. - Cell Physiol.* 275, C1067–C1080. Available at: http://ajpcell.physiology.org/content/275/4/C1067.short.
Hill, T. (1956). A. Fundamental studies. On the theory of the Donnan membrane equilibrium. *Discuss. Faraday Soc.*
Huberfeld, G., Wittner, L., Clemenceau, S., Baulac, M., Kaila, K., Miles, R., and Rivera, C. (2007). Perturbed chloride homeostasis and GABAergic signaling in human temporal lobe epilepsy. *J. Neurosci.* 27, 9866–73. doi:10.1523/JNEUROSCI.2761-07.2007.
Hyde, T. M., Lipska, B. K., Ali, T., Mathew, S. V, Law, A. J., Metitiri, O. E., Straub, R. E., Ye, T., Colantuoni, C., Herman, M. M., Bigelow, L. B., Weinberger, D. R., and Kleinman, J. E. (2011). Expression of GABA signaling molecules KCC2, NKCC1, and GAD1 in cortical development and schizophrenia. *J. Neurosci.* 31, 11088–95. doi:10.1523/JNEUROSCI.1234-11.2011.
Jedlicka, P., Deller, T., Gutkin, B. S., and Backus, K. H. (2011). Activity-dependent intracellular chloride accumulation and diffusion controls GABA(A) receptor-mediated synaptic transmission. *Hippocampus* 21, 885–98. doi:10.1002/hipo.20804.
Jiang, C., and Haddad, G. G. (1991). Effect of anoxia on intracellular and extracellular potassium activity in hypoglossal neurons in vitro. *J. Neurophysiol.* 66, 103–111.
Kaila, K., Price, T. J., Payne, J. a., Puskarjov, M., and Voipio, J. (2014). Cation-chloride cotransporters in neuronal development, plasticity and disease. *Nat. Rev. Neurosci.* 15, 637–654. doi:10.1038/nrn3819.
Kay, A. R. (2017). How Cells Can Control Their Size by Pumping Ions. *Front. Cell Dev. Biol.* 5, 1–14. doi:10.3389/fcell.2017.00041.
Keener, J., and Sneyd, J. (1998). Mathematical Physiology, Interdisciplinary Applied Mathematics 8.
Krishnan, G. P., and Bazhenov, M. (2011). Ionic dynamics mediate spontaneous termination of seizures and postictal depression state. *J. Neurosci.* 31, 8870–82. doi:10.1523/JNEUROSCI.6200-10.2011.
Kuner, T., and Augustine, G. J. (2000). A Genetically Encoded Ratiometric Indicator for Chloride:: Capturing Chloride Transients in Cultured Hippocampal Neurons. *Neuron* 27, 447–459. doi:10.1016/S0896-6273(00)00056-8.
Lagostena, L., Rosato-Siri, M., D'Onofrio, M., Brandi, R., Arisi, I., Capsoni, S., Franzot, J., Cattaneo, A., and Cherubini, E. (2010). In the Adult Hippocampus, Chronic Nerve Growth Factor Deprivation Shifts GABAergic Signaling from the Hyperpolarizing to the Depolarizing Direction. *J. Neurosci.* 30, 885–893. doi:10.1523/JNEUROSCI.3326-09.2010.
Lee, H. H. C., Deeb, T. Z., Walker, J. A., Davies, P. A., and Moss, S. J. (2011). NMDA receptor activity downregulates KCC2 resulting in depolarizing $GABA_A$ receptor–mediated currents. *Nat. Neurosci.* 14, 736–743. doi:10.1038/nn.2806.
Lewin, N., Aksay, E., and Clancy, C. E. (2012). Computational Modeling Reveals Dendritic Origins of GABA A -Mediated Excitation in CA1 Pyramidal Neurons. *PLoS One* 7, 1–17. doi:10.1371/journal.pone.0047250.
Liang, D., Bhatta, S., Volodymyr, G., and Simard, J. M. (2007). Cytotoxic edema : mechanisms of

pathological cell swelling. *Neurosurg Focus* 22, 1–9. doi:10.3171/foc.2007.22.5.3.
Lodish, H., Berk, A., Zipursky, S. L., Matsudaira, P., Baltimore, D., and Darnell, J. (2009). "Intracellular Ion Environment and Membrane Electric Potential," in *Molecular Cell Biology* (New York). Available at: https://www.ncbi.nlm.nih.gov/books/NBK21475/.
Luhmann, H. J., Kirischuk, S., and Kilb, W. (2014). Comment on "Local impermeant anions establish the neuronal chloride concentration." *Science* 345, 1130. doi:10.1126/science.1255337.
MacKenzie, G., and Maguire, J. (2015). Chronic stress shifts the GABA reversal potential in the hippocampus and increases seizure susceptibility. *Epilepsy Res.* 109, 13–27. doi:10.1016/j.eplepsyres.2014.10.003.
Mahadevan, V., Dargaei, Z., Ivakine, E. A., Hartmann, A.-M., Ng, D., Chevrier, J., Ormond, J., Nothwang, H. G., McInnes, R. R., and Woodin, M. A. (2015). Neto2-null mice have impaired GABAergic inhibition and are susceptible to seizures. *Front. Cell. Neurosci.* 9. doi:10.3389/fncel.2015.00368.
Misgeld, U., Deisz, R. a, Dodt, H. U., and Lux, H. D. (1986). The role of chloride transport in postsynaptic inhibition of hippocampal neurons. *Science* 232, 1413–5. doi:10.1126/science.2424084.
Mohapatra, N., Tønnesen, J., Vlachos, A., Kuner, T., Deller, T., Nägerl, U. V., Santamaria, F., and Jedlicka, P. (2016). Spines slow down dendritic chloride diffusion and affect short-term ionic plasticity of GABAergic inhibition. *Sci. Rep.* 6, 23196. doi:10.1038/srep23196.
Nichol, J. A., and Hutter, F. (1996). Tensile strength and dilatational elasticity of giant sarcolemmal vesicles shed from rabbit muscle. *J. Physiol.* 493, 187–198.
Price, T. J., Cervero, F., Gold, M. S., Hammond, D. L., and Prescott, S. A. (2009). Chloride regulation in the pain pathway. *Brain Res. Rev.* 60, 149–170. doi:10.1016/j.brainresrev.2008.12.015.
Qian, N., and Sejnowski, T. J. (1989). An Electro-Diffusion Model for Computing Membrane Potentials and Ionic Concentrations in Branching Dendrites, Spines and Axons. *Biol. Cybern.* 62, 1–15.
Qian, N., and Sejnowski, T. J. (1990). When is an inhibitory synapse effective? *Proc. Natl. Acad. Sci. USA* 87, 8145–8149.
Raimondo, J. V., Joyce, B., Kay, L., Schlagheck, T., Newey, S. E., Srinivas, S., and Akerman, C. J. (2013). A genetically-encoded chloride and pH sensor for dissociating ion dynamics in the nervous system. *Front. Cell. Neurosci.* 7, 202. doi:10.3389/fncel.2013.00202.
Raimondo, J. V., Burman, R. J., Katz, A. A., and Akerman, C. J. (2015). Ion dynamics during seizures. *Front. Cell. Neurosci.* 9, 1–14. doi:10.3389/fncel.2015.00419.
Raimondo, J. V, Richards, B. A., and Woodin, M. A. (2017). Neuronal chloride and excitability — the big impact of small changes. *Curr. Opin. Neurobiol.* 43, 35–42. doi:http://dx.doi.org/10.1016/j.conb.2016.11.012.
Rivera, C., Voipio, J., Thomas-Crusells, J., Li, H., Emri, Z., Sipilä, S., Payne, J. A., Minichiello, L., Saarma, M., and Kaila, K. (2004). Mechanism of activity-dependent downregulation of the neuron-specific K-Cl cotransporter KCC2. *J Neurosci.* 24, 4683–91. doi:10.1523/JNEUROSCI.5265-03.2004.
Rungta, R. L., Choi, H. B., Tyson, J. R., Malik, A., Dissing-Olesen, L., Lin, P. J. C., Cain, S. M., Cullis, P. R., Snutch, T. P., and Macvicar, B. A. (2015). The cellular mechanisms of neuronal swelling underlying cytotoxic edema. *Cell* 161, 610–621. doi:10.1016/j.cell.2015.03.029.
Sachs, F., and Sivaselvan, M. V (2015). Cell volume control in three dimensions: Water movement without solute movement. *J. Gen. Physiol.* 145, 373–380. doi:10.1085/jgp.201411297.
Savtchenko, L. P., Poo, M. M., and Rusakov, D. A. (2017). Electrodiffusion phenomena in neuroscience: a neglected companion. *Nat. Publ. Gr.* 18, 598–612. doi:10.1038/nrn.2017.101.
Sperelakis, N. (2012). "Chapter 10 – Gibbs–Donnan Equilibrium Potentials," in *Cell Physiology Source Book*, 147–151. doi:10.1016/B978-0-12-387738-3.00010-X.
Staley, K. J., and Proctor, W. R. (1999). Modulation of mammalian dendritic $GABA_A$ receptor function by the kinetics of Cl- and HCO3- transport. *J. Physiol.* 519, 693.
Tang, D., Qian, A., Song, D., Ben, Q., Yao, W., Sun, J., Li, W., Xu, T., and Yuan, Y. (2015). Role of the potassium chloride cotransporter isoform 2-mediated spinal chloride homeostasis in a rat model of visceral hypersensitivity. *Am. J. Physiol. Gastrointest. Liver Physiol.* 308, G767-78. doi:10.1152/ajpgi.00313.2014.

963 Tosteson, D. C., and Hoffman, J. F. (1960). Regulation of cell volume by active cation transport in high
964 and low potassium sheep red cells. *J. Gen. Physiol.* 44, 169–194.
965 Tyzio, R., Ivanov, A., Bernard, C., Holmes, G. L., Ben-Ari, Y., and Khazipov, R. (2003). Membrane
966 potential of CA3 hippocampal pyramidal cells during postnatal development. *J. Neurophysiol.* 90,
967 2964–72. doi:10.1152/jn.00172.2003.
968 Tyzio, R., Minlebaev, M., Rheims, S., Ivanov, A., Jorquera, I., Holmes, G. L., Zilberter, Y., Ben-Ari, Y., and
969 Khazipov, R. (2008). Postnatal changes in somatic gamma-aminobutyric acid signalling in the rat
970 hippocampus. *Eur. J. Neurosci.* 27, 2515–28. doi:10.1111/j.1460-9568.2008.06234.x.
971 Tyzio, R., Nardou, R., Ferrari, D. C., Tsintsadze, T., Shahrokhi, A., Eftekhari, S., Khalilov, I., Tsintsadze,
972 V., Brouchoud, C., Chazal, G., Lemonnier, E., Lozovaya, N., Burnashev, N., and Ben-Ari, Y. (2014).
973 Oxytocin-mediated GABA inhibition during delivery attenuates autism pathogenesis in rodent
974 offspring. *Science* 343, 675–9. doi:10.1126/science.1247190.
975 Verkman, A. S. (2002). Solute and macromolecule diffusion in cellular aqueous compartments.
976 *TRENDS Biochem. Sci.* 27, 27–33.
977 Voipio, J., Boron, W. F., Jones, S. W., Hopfer, U., Payne, J. a, and Kaila, K. (2014). Comment on "Local
978 impermeant anions establish the neuronal chloride concentration". *Science* 345, 1130.
979 doi:10.1126/science.1252978.
980 Xiao, A., Wei, L., Xia, S., Rothman, S., and Yu, S. (2002). Ionic mechanisms of ouabain-induced
981 concurrent apoptosis and necrosis in individual cultured cortical neurons. *J. Neurosci.* 15, 4.
982 doi:22/4/1350 [pii].
983 Yeh, B. K., and Lazzara, R. (1973). Reversal of Ouabain-lnduced Electrophysiological Effects by
984 Potassium Canrenoate in Canine Purkinje Fibers. *Circ. Res.* 32, 501–508.
985 doi:10.1161/01.RES.32.4.501.
986